Reprinted from The Journal of Physical Chemistry, 1995, 99.

Ultrafast Measurements of Chemistry in Clusters: Excited-State Proton Transfer

Jack A. Syage

The Aerospace Corporation, P.O. Box 92957/M5-754, Los Angeles, California 90009

Received: November 23, 1994[⊗]

In this article we report on the progress being made in understanding solvent interactions at the molecular level from time-resolved studies of chemistry in clusters. We begin by reviewing the variety of reactions studied in clusters by time-domain techniques. We then focus our discussion on the prototype hydrogen-bonded system ROH·B_n, where ROH is an aromatic alcohol such as phenol or naphthol and B_n is a cluster of solvent molecules. This system undergoes excited-state proton transfer and is important because it is being investigated on many fronts, e.g., dynamical, spectroscopic, and structural determinations, in clusters, and in condensed phase, along with supporting theoretical work. We review results that show a strong dependence of reaction rate on solvent type, size, and structure, in pure and binary solvents. Solvent dynamics such as structural reorganization following proton transfer are also evident. These properties, along with deuteration experiments, are indicating a tunneling mechanism for proton transfer. The effect of individual solvent molecules on the barrier properties and product energies is discussed and compared to condensed-phase studies. Throughout our discussion we take the opportunity to inject some speculation and opinion regarding future directions, outstanding issues, and conflicting results.

1. Introduction

It is almost a cliche to say that a field is growing by leaps and bounds and that great progress has been made in understanding fundamental properties of matter. However, this statement certainly rings true for the field of clusters. Clusters are an ideal medium for understanding the connection between gas-phase and condensed-phase phenomena and in learning about the breakdown of bulk-phase properties as a system becomes increasingly smaller in size. The structure of the solvent about a reacting molecule is a longstanding issue, and the interactions exerted by the solvent often determine the fate of chemical reactions. In this review we discuss how cluster studies are contributing to an understanding of how solvent molecules control chemical reactions. This article complements a number of review articles that cover the general topic of chemistry in clusters.[1-3]

There is currently great interest in developing techniques for controlling chemical reactions by laser methods involving mode specificity or coherent control.[4-6] Still the most practical way to manipulate large-scale chemistry is to vary solvent conditions. The synthetic chemist relies on known procedures for choosing solvent conditions; however, this knowledge is usually gained empirically. Learning about solvent interactions in greater detail could potentially lead to important advances in the control of bulk-phase chemistry. Measurements in the bulk phase are certainly important for testing solvent effects; however, many details are lost because of the averaging of solvent configurations and energy distributions (canonical ensemble). Cluster experiments, on the other hand, permit measurements for specific solvent interactions, in specific geometries, at specific energies (microcanonical ensemble). Researchers of cluster and bulk-phase properties are working more closely together to discover new correspondences between these phases of matter.

Measurements of cluster dynamics in the time domain began with Felker and Zewail who measured the picosecond dynamics of hydrogen-bond dissociation for the stepwise solvation of isoquinoline.[7] Today there are many groups conducting real-time measurements in clusters encompassing a large scope of interests.[7-38] These range from the study of chemical reactions,[9-30] which is the subject of this article, to vibrational relaxation and van der Waals dissociation,[6-9,31-35] to coherent oscillations and cage effects,[9-12] to structural analysis using rotational coherence spectroscopy.[36,37] With regard to chemistry studies, two classes of reactions are becoming prototype systems: (i) excited state proton transfer (ESPT) of aromatic acids such as phenol and naphthol[14-23,38-41] and (ii) dissociation/recombination cage dynamics of molecules such as I_2 (or I_2^-).[9-12,42,43] What adds value to these studies is that a corresponding literature exists for these reactions in the condensed phase. Below we summarize the variety of reactions that have been investigated in the time domain. In the main body of the article we focus on the ESPT problem.

In our laboratory we have been interested in the picosecond dynamics of ESPT of phenol (PhOH) complexed to a variety of solvents.[17-23] Several issues have been investigated: solvent dependence on rate,[17] cluster ion properties,[18] ESPT in phenol dimers,[19] structural effects,[19] photoelectron studies of solvent reorganization,[21] and the mechanism of proton tunneling.[22] The Zewail group[14,15] and the Bernstein and Kelley group[16] have been studying similar properties for naphthol (NpOH). These studies have recently been extended by Zewail and co-workers to the femtosecond domain.[15] These investigators found that for 1-NpOH$(NH_3)_n$ the minimum number of solvent molecules necessary to observe ESPT is $n = 3$. Our measurements for PhOH$(NH_3)_n$ gave a corresponding value of $n = 5$. The difference in the critical ammonia solvent size for ESPT for phenol vs 1-naphthol is consistent with the difference in acidity of the two S_1 excited aromatic acids (pK_a of 4.1 and 0.5,

[⊗] Abstract published in *Advance ACS Abstracts,* April 1, 1995.

0022-3654/95/2099-5772$09.00/0

respectively[44]). In a related series of experiments Brucker and Kelley measured proton-transfer rates in small solvent complexes formed in cryogenic argon matrices.[45] They observed similar solvent size dependences for 1-naphthol−ammonia; however, the rates differed from that of the isolated clusters formed in molecular beams, presumably due to the polarizability of the Ar matrix. The above studies, which we discuss in greater detail later in this paper, are important because they can be related to the large literature of ultrafast studies of ESPT in solution by the groups of Robinson,[46] Barbara,[47] Huppert and Gutman,[48−50] Clark,[51] Kelley,[52] and others.

Another cluster system that has become a prototype for measuring solvent caging of a photodissociation is I_2-M_n. The history of dissociation and cage recombination studies of I_2 began in the condensed phase in the groups of Eisenthal[53] and Wilson,[54] followed by the groups of Kelley[55] and Harris.[56] Two exciting results relating neutral I_2 dissociation/recombination in clusters and solids have recently been reported respectively by Zewail and co-workers[11] and by Apkarian, Martens, and co-workers[57] using rare gas atoms as the solvent cage. In these studies the solvent or matrix potential barrier is directly probed and the extent of lattice excitation measured. Lineberger's group carried out intricate caging experiments on $I_2^-(CO_2)_n$.[9,10,58] These investigators observed nearly complete caging for $n \geq 16$ and observed an interesting recurrence at 2 ps. For smaller cluster sizes the cage probability decreased nearly monotonically with decreasing n. Barbara and co-workers measured I_2^- dissociation/recombination dynamics in liquid solvents, thus providing a connection between cluster and bulk liquid phenomena.[59] In a related experiment, Ruhman and co-workers observed coherent vibrational motion of I_2^- resulting from I_3^- photodissociation in the condensed phase.[60] In our laboratory we measured the formation of I_2 from two different molecules by initiating intermolecular chemistry in clusters. The photodissociation of $CH_3I \rightarrow CH_3 + I$ in CH_3I clusters leads to fast radical chemistry and formation of intermediate species that ultimately form the stable products $C_2H_6 + I_2$.[24] The kinetic energy of escaped I atom was also measured and shows considerable collisional quenching of translational energy relative to the photodissociation of isolated CH_3I molecules.[25]

Ultrafast studies of clusters have been applied to other types of reactions that we will not cover in detail in this review. Recently, Castleman and co-workers measured femtosecond reaction dynamics for excitation to the dossociative $\tilde{A}$ state and predissociative $\tilde{C}'$ state in ammonia clusters.[26] They were able to distinguish two pathways to protonation from the excited-state clusters: ionization followed by ion dissociation of NH_2 *vs* neutral dissociation of NH_2 followed by ionization. Fuke *et al.* measured the picosecond proton transfer rate in 1-azacarbazole dimer and observed a strong mode-specific acceleration of rate for the symmetric intermolecular N−H···N stretch vibration.[27] We will have more to say about this intriguing result later in discussion of a tunneling mechanism for ESPT. The groups of Wittig[28] and Soep[29] have championed the method of aligning bimolecular collision partners in van der Waals dimers. These groups have followed Zewail and co-workers[30] in extending these studies into the picosecond and femtosecond time domain. The photodissociation of HI in the CO_2−HI complexes to form OH is an excellent example of the detailed information on reaction dynamics obtained by alignment-, time-, and state-resolved measurements in complexes.[28−30] Finally, a growing body of literature is concerned with the time evolution of van der Waals dimer dissociations.[7−11,31−35]

Though the focus of this article is on ultrafast measurements in clusters, we make connections to related studies, *e.g.*, structural analysis and condensed-phase measurements, in order to better learn about the role of solvent in chemistry in the broadest sense. We also take the opportunity to inject some speculation and opinion regarding future directions, outstanding issues, and conflicting results.

2. Experimental Methods

Excitation and Detection. In a typical pump−probe experiment, chemistry is initiated by a photoexcitation pulse, and the evolution of cluster properties is interrogated at later times by probe excitation. The more common probe excitation methods include mass- and/or photoelectron-detected ionization, mass-detected ion photofragmentation, or fluorescence excitation sometimes employing stimulated emission or fluorescence depletion. One should refer to original articles for details on experimental and pump−probe optical layouts. We give brief descriptions here. In our laboratory,[17,23] a number of possible choices for the pump and probe pulses are available from the Nd:YAG harmonics and the dye laser. (The later employs the usual wavelength extension capabilities, *e.g.*, doubling, mixing, and Raman shifting.) One arrangement uses the Nd:YAG harmonics, 266 nm as the pump, and 532 nm (or 355 nm) as the probe. The other arrangement uses tunable UV output from the dye laser as the pump and 355 nm as the probe. We employ other combinations on occasion for both cluster and noncluster work (*i.e.*, 266 nm + vis, UV + 532 nm, UV + vis). Our picosecond, Nd:YAG laser employs a pulsed mode-locked oscillator that operates at 10−20 Hz. A single pulse from the pulse train is extracted and amplified. The Nd:YAG second harmonic at 532 nm (about 20 mJ/pulse and 20 ps duration) is used to pump the tunable dye laser oscillator and amplifiers. The oscillator yields tunable pulses of several nanojoules that pass through four stages of dye amplification to give 1−2 mJ pulses of 5−8 ps duration.

Molecular Beam Mass Spectrometry. The most common detection schemes for neutral cluster molecular beam experiments are photoionization mass spectrometry, photoelectron spectroscopy, and fluorescence excitation. For cluster ion experiments it is customary to mass-select a specific cluster size before pump−probe excitation and then detect characteristic fragment ions resulting from probe excitation. A standard molecular beam time-of-flight (TOF) mass spectrometer, as depicted in Figure 1A, employs two chambers. The first chamber contains a pulsed supersonic nozzle. A skimmer mounted at the interface of the two chambers allows only the central portion of the expansion to pass into the second chamber, giving a reasonably collimated molecular beam. The molecular beam is then crossed by the laser in an ion optics assembly used to accelerate ions into a TOF drift tube. Clusters that are ionized by the probe pulse are mass-analyzed in the TOF mass spectrometer. In our molecular beam apparatus in Figure 1A we also employ a pulsed electron gun to measure ionization cross sections in cluster and noncluster experiments,[61,62] to monitor cluster distributions as a function of pulsed valve conditions, and to measure thermochemical thresholds for cluster ion fragments. Finally, a combination of EI ionization, mass filtering, and laser photodissociation is used to measure size-specific electronic spectra and fragmentation mechanisms of cluster ions.[63,64]

Molecular Beam Photoelectron Spectroscopy. Time-resolved photoelectron spectroscopy (TR-PES) has recently been applied to cluster studies.[21,31,33] The two most common methods are TOF and threshold photoelectron spectroscopy. In the former case a single ionization wavelength is used, and a distribution of photoelectron energies is dispersed by their drift

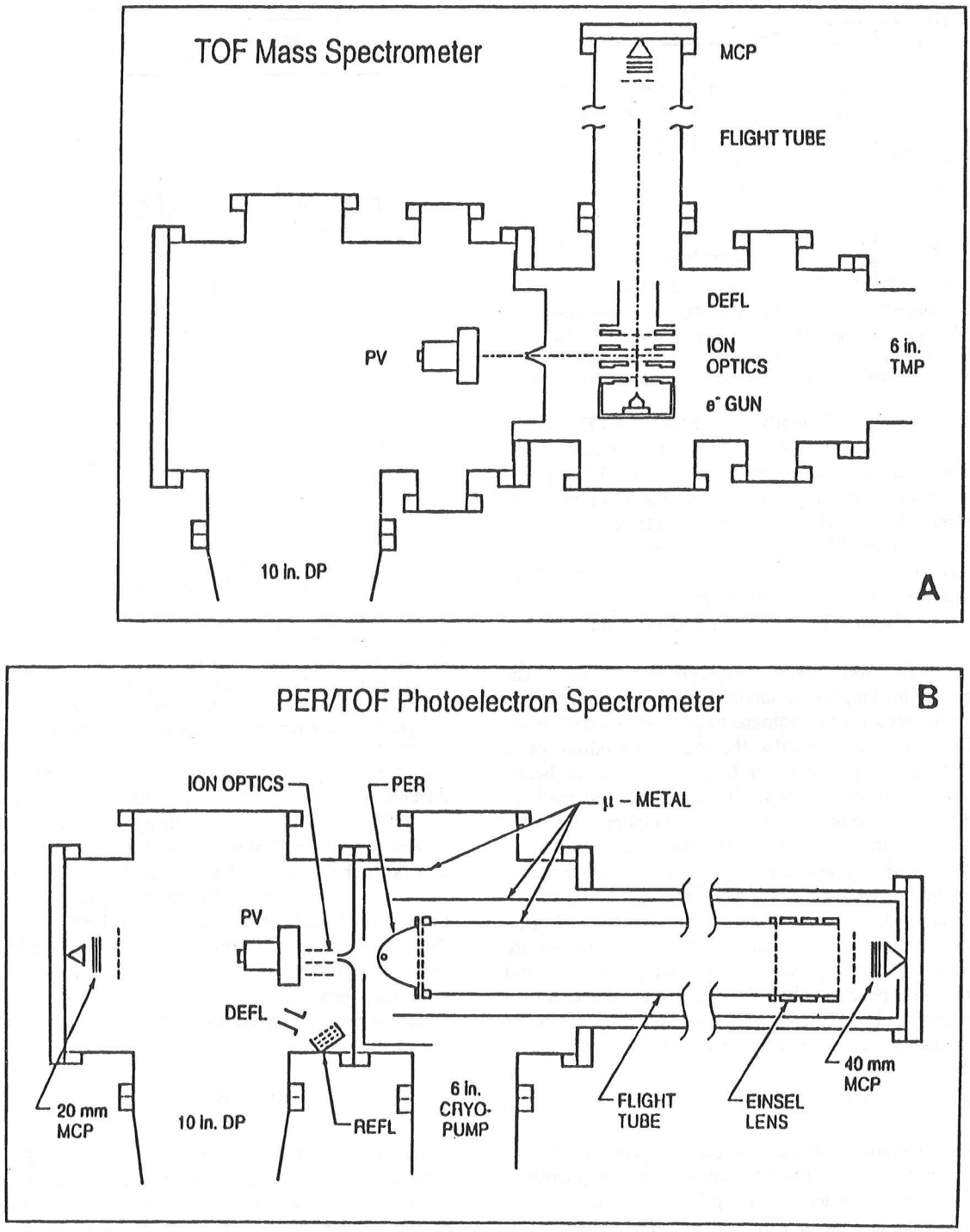

Figure 1. Experimental schematic: (A) molecular beam mass spectrometer; (B) molecular beam photoelectron spectrometer. Terms are defined as follows: DEFL, deflector plates; DP, diffusion pump; MCP microchannel plate detector; PER, paraboloidal electrostatic reflector; PV, pulsed valve; REFL, reflecting grids; TMP, turbomolecular pump. The laser beam crosses orthogonally with the molecular beam at the intersection with the flight tube axis in the mass spectrometer and through holes in the side of the PER in the photoelectron spectrometer.

times to a detector. In the latter case, referred to as zero kinetic energy pulsed field ionization (ZEKE-PFI), the ionization wavelength is scanned, and ion thresholds are detected by the collection of near zero kinetic energy electrons.[65] In TOF photoelectron spectroscopy a nontunable ionization pulse can be used, and all photoelectron energies are detected instantly; however, the energy resolution has a limit of about 10 meV (about 80 cm^{-1}). In ZEKE-PFI, a tunable laser is needed for ionization, and only one threshold is detected at once; however, the energy resolution is far superior (better than 1 cm^{-1}). Furthermore, this technique is easily adapted for mass-analyzed threshold ionization (MATI),[66,67] which is an important feature for achieving mass specificity in cluster studies. The Knee group has measured intramolecular vibrational redistribution (IVR) and vibrational predissociation of van der Waals bonds by picosecond ZEKE-PFI.[31]

Our group has made picosecond measurements of ESPT and solvent dynamics in clusters using a variant of TOF photoelectron spectroscopy that uses a paraboloidal electrostatic reflector as shown in Figure 1B.[21,68] The PER reflects and collimates electrons that would otherwise disperse through a large distribution of angles. Nearly 2 orders of magnitude improvement in collection efficiency is obtained over direct line-of-sight electron detection.[68,69] An alternative electron-collimating device is a

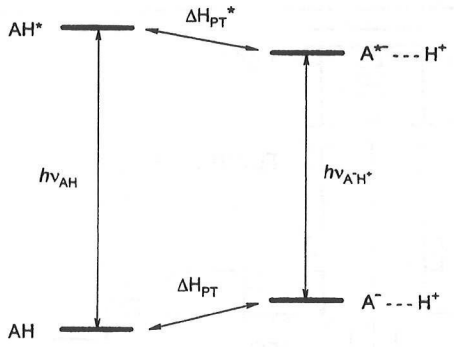

Figure 2. Generalized Förster diagram. The transition energies of the neutral and ion pair are denoted as $h\nu_{AH}$ and $h\nu_{A^-H^+}$. The latter emission is due mostly to the conjugate base A^-. ΔH_{PT} is the enthalpy of proton transfer, and the asterisk denotes excited electronic state.

magnetic bottle.[70,71] Currently, our PER/TOF-PES cannot identify the ion mass corresponding to the photoelectron. We have some capacity for detecting mass-selective PES spectra by simultaneously recording ion mass spectra (chamber I) and PES spectra (chamber II). However, a preferred method of mass-analyzed TOF-PES is to use photoelectron−photoion coincidence (PEPICO),[71] which lends itself nicely to a high repetition mode-locked laser, provided pulse energy is increased by some scheme such as cavity dumping, Q-switching, or pulse amplification.

Mass-Selected Ion Beam Photofragmentation. The Lineberger group employs a tandem mass spectrometer apparatus for time-resolved measurements of mass-selected cluster ions.[9] Cluster ions are formed at the source of a pulsed valve by crossing the free jet expansion by a 1 keV electron beam. The cluster ions grow in size in the expansion and then are allowed to drift before being extracted into a tandem TOF mass spectrometer. In the linear TOF stage, the cluster ion masses separate and a pulsed mass gate allows a single mass through. Laser excitation occurs just beyond this region. The resultant parent ion and fragment ions and neutrals then enter a reflectron TOF. The reflectron acts as a filter in which fragment ions are reflected and detected by one detector and parent ions and neutral fragments penetrate the reflectron and are detected by a second detector. The Johnson group at Yale uses a similar device for studying S_N2-type reactions in cluster ions.[72]

3. Excited-State Proton Transfer

3.1. Background. Aromatic alcohols tend to be more acidic in their S_1 state than in S_0. Photoexcitation, therefore, increases acidity, giving rise to the term pH jump.[49] The Förster diagram in Figure 2 helps to explain why this is.[73] The difference in the heat of deprotonation ΔH_d for the ground and excited electronic states of an acid AH is determined by the difference in the electronic transition energy of AH vs the conjugate base A^-. For aromatic alcohols, the AH transition energy is greater than that of A^-, leading to a greater acidity for AH* than for AH. This property can be understood in more detail by studying the highest occupied and lowest unoccupied molecular orbitals (HOMO and LUMO) of AH and A^-.[74] It is generally true that excited electronic states lie at lower energy for transitions involving unpaired electrons than for paired electrons, which is consistent with the above notions.

Excited-state proton transfer (ESPT) reactions have been studied extensively in the condensed phase including several time-resolved experiments.[46−52] These reactions are strongly solvent dependent, which can be understood by examining the Förster diagram in Figure 2. The neutral acid AH (or AH*)

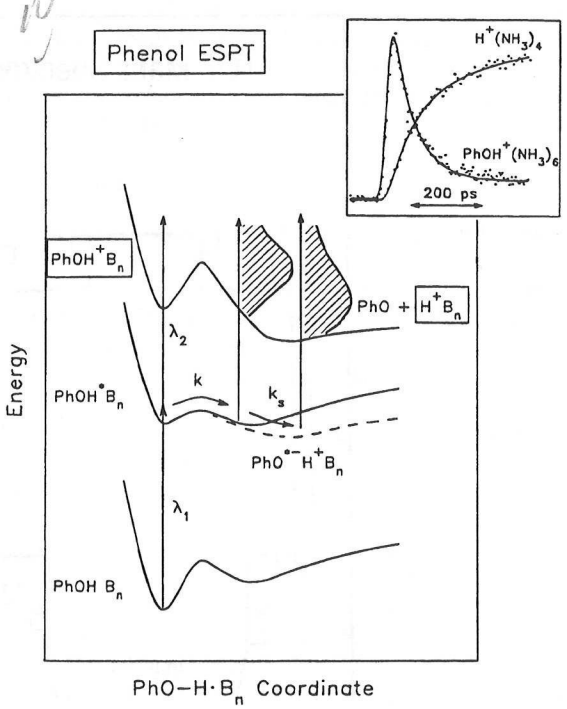

Figure 3. Schematic energy diagram for $PhOH(NH_3)_n$ (consistent with $n \sim 5$). The pump and probe pulses are denoted as λ_1 and λ_2, and the excited-state proton transfer and solvent reorganization rate constants are given by k and k_s, respectively. Approximate photoelectron band shapes are shown by the shaded areas. The ion signals for reactant and product are given in the insert and show matching kinetics.

and the conjugate base A^- (or A^{*-}) tend to be stabilized differently by the solvent, which means that the acidities of the ground and excited states can change markedly with different solvents. A solvent that is polar or that has a high proton affinity will favor the dissociated acid over the undissociated acid.

The first study of ESPT in a cluster was reported by Leutwyler, Cheshnovsky, and co-workers for 1-naphthol−$(NH_3)_n$.[39,40] These experiments were important because they showed that it is possible to investigate how individual solvent molecules progressively stabilize the product states. We represent proton transfer from the aromatic acid ROH (R = naphthyl or phenyl) by the following

$$ROH^*B_n \xrightarrow{k} RO^{*-}H^+B_n \qquad (1)$$

which corresponds to a conversion from a locally excited S_1 state with a covalent O−H bond to an excited ion-pair state. B_n refers to the solvent cluster consisting of n molecules of base B. The first experiments made use of steady-state mass spectra and emission spectra using nanosecond excitation. Leutwyler's group obtained evidence for a threshold for reaction for ammonia solvation of $n = 4$. Solgadi *et al.* measured steady-state threshold ionization curves for phenol−$(NH_3)_n$ and also reported an ESPT threshold of $n = 4$,[41] even though phenol is a weaker acid than naphthol. Time-resolved measurements were reported by the Zewail group[14,15] and the Bernstein and Kelley group[16] for 1-naphthol and by our group for phenol[17−23] using various solvents.

A qualitative picture of the cluster potential energy curves for ground, excited, and ionic states is given in Figure 3 along with the picosecond pump−probe excitation/detection scheme used to measure the chemical rates. Figure 3 also shows representative ion energy distributions, measurable by photoelectron spectroscopy (described in section 3.4). Reactant and product are distinguishable in our experiments on phenol by

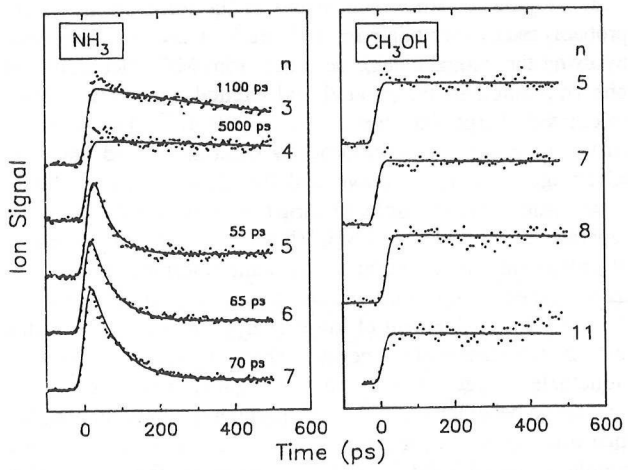

Figure 4. Picosecond measurements of PhOH*B_n for B = NH_3 and CH_3OH using 266 nm pump and 532 nm, probe. The calculated curves for CH_3OH solvation assume a lifetime of 10 ns.

mass spectrometry because they fragment differently upon ionization.[17,18] Ionization of reactant clusters PhOH*···B_n produces cluster ions PhOH$^+$···B_n on the inner potential well where the O−H coordinate is strongly bound. Conversely, ionization of the product ion pairs PhO*$^-$···H^+B_n produces cluster ions PhO···H^+B_n on the outer well where facile dissociation occurs to give H^+B_n. The observed reactant and product signals show matching kinetics, which is important for establishing that the observed response is a proton transfer reaction. The propensity for the excited-state reactant and product to fragment differently upon ionization apparently is not observed for the 1-naphthol experiments by Zewail *et al.*[14,15] and by Bernstein and Kelley *et al.*[16]. Under their excitation conditions, the reactant kinetics is observable because the ionization efficiency from product is considerably less than for reactant.

3.2. Basicity and Solvent Size Dependence. *Experimental Measurables.* There is now a fairly large collection of rate measurements for phenol and 1-naphthol in a variety of solvent clusters from which to learn about fundamental interactions of solvent molecules. Figures 4 and 5 show a series of excited-state reactant decay curves for these two systems. The phenol results in Figure 4, recorded in our laboratory, show a distinct onset to reaction at $n = 5$ ammonia molecules.[17,23] The 1-naphthol results in Figure 5 from the Zewail laboratory show a threshold at $n = 3$.[14,15] A similar conclusion in the latter case was reached for measurements by Bernstein, Kelley, and co-workers.[16] The pK^*_a values (*i.e.*, the negative logarithm of the equilibrium constant K_a for acid dissociation) of excited state 1-naphthol and phenol are 0.5 and 4.1, respectively, which converts to an enthalpy difference of 0.22 eV.[44] Thus, additional ammonia solvent molecules are required to stabilize ESPT in phenol compared to 1-naphthol. If the rates of ESPT for NH_3 solvation in Figures 4 and 5 are plotted versus n, the resulting curve takes on a shape and inflection that is reminiscent of an acid−base titration curve. Indeed, mass-specific, time-resolved cluster experiments correspond to *single molecule titration* measurements.

Measurements of ESPT in other solvents show striking differences compared to ammonia solvation. In Figure 4 no reaction is observed for phenol$(CH_3OH)_n$ up to $n = 11$. Water is also inactive for these moderate cluster sizes for phenol and for 1-naphthol. Knochenmuss *et al.* report reaction occurring in 1-naphthol$(H_2O)_n$,[38] but the thresholds are several hundred water molecules and the rates are on the nanosecond, not picosecond, time scale. For more basic solvent molecules, small solvent size thresholds for reaction are observed. In phenol, ESPT was observed for trimethylamine solvent at $n = 3$ and for hydrazine at $n = 5$.[17] In 1-naphthol a reaction was observed at $n = 2$ for piperidine solvent.[15] In the next subsection on solvent structure (section 3.3), we will present unusual behavior observed in mixed solvents.

How do these cluster rates compare to condensed-phase measurements? The ESPT lifetimes in PhOH and 1-NpOH in ammonia are in the 20−100 ps range depending on vibrational energy. No measurements in bulk ammonia have yet been

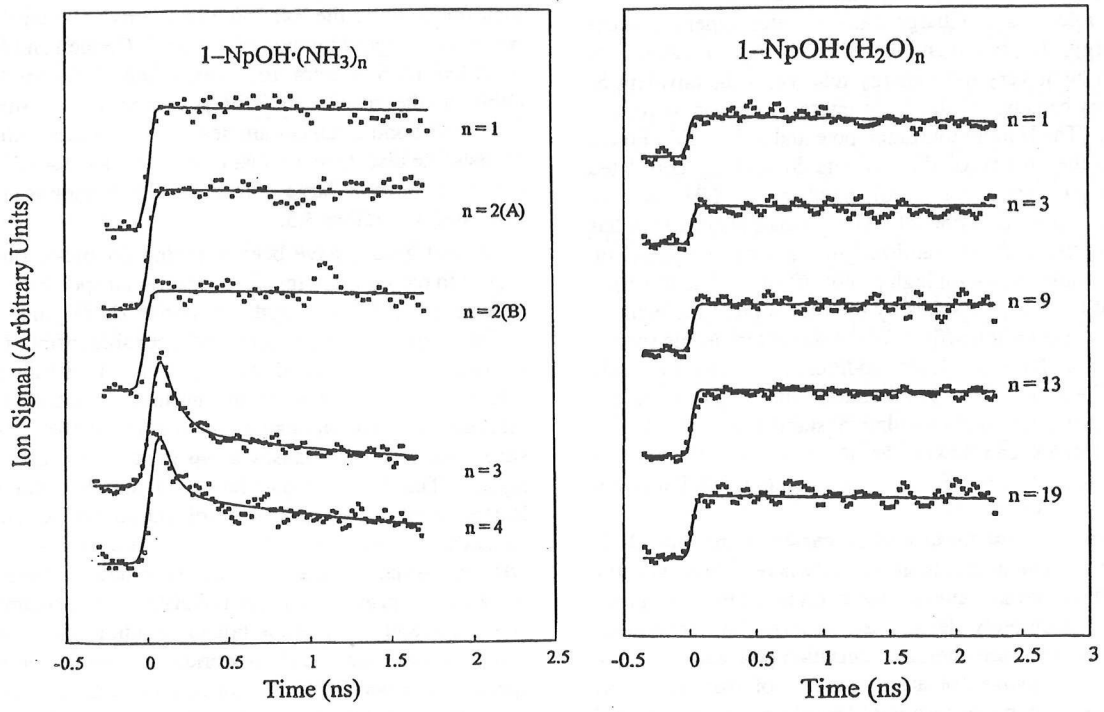

Figure 5. Picosecond measurements of 1-NpOH*B_n for B = NH_3 and H_2O. 2 (A) and 2 (B) refer to different geometries for $n = 2$ ammonia molecules. Pump excitation was near the S_1 origin, and probe excitation was near the ionization threshold. (Results are from refs 14 and 15.)

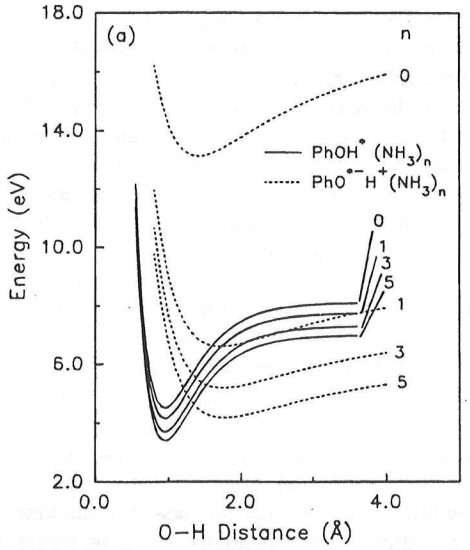

Figure 6. Approximate $PhOH(NH_3)_n$ cluster potential energy curves for the reactive PhO−H coordinate. These curves assume an equilibrium O···N bond distance (approximately 1.8 and 1.0 Å for the neutral and ion-pair states, respectively).

made. In water solution, the groups of Robinson and Clark measured room temperature lifetimes of about 40 ps for 1-NpOH.[46,51] In other condensed-phase systems, the ESPT rate is over an order of magnitude slower for 2-NpOH in water or for 1-NpOH in methanol or ethanol. Interestingly, 1-NpOH is unreactive in small water clusters and only becomes reactive on a nanosecond time scale for a cluster of several hundred water molecules according to the study of Knochenmuss *et al.*[38] The difference in the cluster and condensed-phase results is probably attributable to temperature. This is a parameter that needs to be dealt with better in cluster systems in order to make more meaningful comparisons to the condensed phase.

Energetics. The results presented so far are sufficient to begin examining the energetics of stepwise solvation. Our starting premise is that ion-pair or proton-transfer states in clusters (or condensed phase) are associated with charge-transfer states in gas-phase molecules.[17] Charge-transfer states generally occur at high energy. In phenol and naphthol, the relevant states are expected to lie at very high energy relative to the covalent S_0 and S_1 states because of the large energy required to form a free proton. (The H atom ionization potential is 13.6 eV.) Figure 6 compares the energy of the covalent S_1 and the correlated excited ion-pair state for small numbers of NH_3 solvent molecules complexed to phenol. The ion-pair state, which has large proton character, is stabilized strongly by complexation of phenol to molecules with high proton affinity. The lowering in energy of the ion-pair states by the first solvent molecule is comparable to the proton affinity of the solvent molecule (which is 8.8 eV for NH_3[75]). Each additional solvent molecule contributes less and less stabilization (the stepwise proton affinity[76]); however, the cumulative stabilization by a few solvent molecules can lower the ion-pair state to energies comparable to that of the S_1 state, thus making ESPT thermodynamically allowed.

The details of how these energy curves along the O−H coordinate were calculated is given elsewhere;[17] however, the basic ingredients are as follows. The energies of the asymptotic limits can be accurately determined because they depend on known bond dissociation energies, ionization potentials, electron affinities, and stepwise solvation energies of bare H^+. The reactant covalent bond is described by a Morse potential, and the product ion-pair bond is described by a Coulomb potential with a repulsive term. The shapes of the ion-pair curves are probably the least certain part of Figure 6. They were calculated by using theoretical charge densities from MO calculations of phenoxy anion in the ground and excited states[74] and from calculated charge densities for $NH_4^+(NH_3)_n$.[77] The potential curves in Figure 6 are empirically determined and have the advantage of being intuitive and the disadvantage of being nonrigorous. For example, treating the charges as fixed for the separate entities PhO^- and $NH_4^+(NH_3)_n$ neglects the possibility of charge flow in the complex by some intermolecular polarizability mechanism. Furthermore, this simple model overlooks the possible involvement of lower energy polar aromatic states and the stabilization of the negative charge by solvent molecules. Nonetheless, Figure 6 is instructive because it captures all the qualitative behavior observed in experiments. In particular, the measured threshold for NH_3 solvation agrees closely with the simple potential model, lending support to the notion that solvation of high-energy ion-pair states is the mechanism of acid−base chemistry in condensed phase.

3.3. Solvent Structure. *Structure Analysis from Spectroscopy.* The study of chemistry in clusters affords the opportunity to measure reaction rates for specific cluster sizes and configurations. However, experimental means are needed to determine the structure of clusters. Important spectroscopic tools have recently been developed to determine structure. High-resolution electronic state excitation spectra (detected by ionization or fluorescence) have been employed by the groups of Pratt,[78,79] Levy,[80] and Leutwyler,[81] primarily to determine rotational constants from which geometry can be deduced. Felker and Zewail obtain similar information from the time-domain technique called rotational coherence spectroscopy (RCS).[36,37,82] The frequency domain techniques require well-resolved spectra and are, therefore, better suited to smaller clusters. The RCS technique is less restrictive of spectral congestion because it does not measure spectral features, but rather rotational recurrences, which occur at intervals related to the rotational constants. Spectral congestion becomes a limitation only when the spectra of different cluster sizes overlap; then ion-detected RCS becomes necessary. Pratt *et al.* determined structure from measurements of the rotational constants of 1- and 2-naphthol bound to a single ammonia molecule.[79] Connell and Felker have recorded RCS spectra for 1-naphthol$(NH_3)_n$ up to $n = 3$, although the results are still preliminary.[82] Values for the O−H···N bond distances are now being reported although there exists some discrepancies that require further study.[83] The bond distances have a large effect on the tunneling rates as is discussed in section 3.5.

Several groups have been applying double-resonance techniques to record mass-resolved vibrational spectra. In the basic scheme a fixed-wavelength ultraviolet (UV) pulse resonantly ionizes a specific cluster size, and a tunable infrared (IR) pulse or two-color stimulated Raman pulse is scanned through vibrational absorptions of the ground electronic state. The vibrational transitions cause a depletion of the initial ground state, which in turn causes a dip in the resonance ionization signal. The Felker group has used ion detected stimulated Raman spectroscopy to record solvent vibrational structure for benzene complexed with N_2.[84] For hydrogen-bonded systems, OH vibrational spectra have been recorded for benzene$(H_2O)_n$ by Zwier's group[85] for phenol$(H_2O)_n$ by Mikami and co-workers[86] and for phenol bound to other molecules in 1:1 complexes by Felker and co-workers.[87a] So far, no vibrational spectra have been reported for ammonia molecules bound to an aromatic molecule for larger than 1:1 complexes, although experiments are currently in progress for 1-naphthol$(NH_3)_n$.[87b]

From a dynamics point of view, there are many structural properties of the solvent that need to be addressed, for example: (1) Where do solvent molecules bond to molecules such as phenol and naphthol? (2) What are the hydrogen bond properties such as O−H and H−X distance and O−H−X angle, where X is a solvent heteroatom? (3) How do these structures change between ground and excited states and between neutral and ion-pair forms (*i.e.*, undissociated and dissociated acid forms)?

For phenol$(H_2O)_n$, water forms a self-associated hydrogen bond network that builds off the phenol hydroxy proton, but which makes attachments with the O atom and the ring as n increases. Several studies indicate that a cyclic structure occurs for $n = 2$.[86−89] Recently, Mikami provided evidence for a zwitterionic structure for the solvent for $n \geq 4$.[86] However, Zwier interprets similar spectral features in benzene$(H_2O)_n$ as a branching into a Y structure in what he terms a double donor structure.[85] The big question for ammonia solvation is whether a similar self-associated chain structure builds off the aromatic hydroxy or do some solvent molecules bind independently to the ring. Most studies indicate that the first ammonia binds to the hydroxy proton, at least for phenol, since the ROH−NH_3 bound is greater than the ring−NH_3 bond strength (about 0.29 eV *vs* about 0.15 eV, respectively).[17,90,91] Calculations by Bernstein *et al.*, however, indicate that ammonia bonds more favorably to the ring than to the hydroxy group, at least for naphthol.[92] It is plausible that the second ammonia would bond to the ring after the first bonds to the hydroxy since the ring bond energy is about the same as the NH_3−NH_3 dimer bond energy of 0.15 eV. Preliminary measurements by Felker *et al.* suggest that the second ammonia bonds to the first ammonia; however, for $n = 3$ there may be an isomer for which one ammonia bonds to the ring.[82] The bonding sites of ammonia is a core issue because it bears directly on the mechanism of ESPT stabilization, such as, what is the relative importance of proton *vs* anion stabilization?

Structure Analysis from Dynamics. Unfortunately, structure determinations by spectroscopic measurements are difficult for reacting cluster systems because the spectra are usually very diffuse. A number of other means have been employed to extract structural information on clusters, such as (i) observing particularly stable clusters in mass spectra,[93,94] (ii) by measuring the fragmentation patterns of clusters,[95,96] and (iii) by introducing chain-terminating hydrogen-bonding molecules to determine the number of available hydrogen-bonding sites.[19,97] These techniques alone may not give definitive results, but collectively, and in combination with other information, they can dramatically reduce the number of possible structures under consideration. We have found these approaches quite useful in our cluster studies and will present some examples of structure elucidation for phenol in neat and mixed solvents.

First, we address the crucial issue of the NH_3 binding sites. As discussed above, we time-resolve both excited-state reactant and product by detecting the ionized signals $PhOH^+(NH_3)_n$ and $H^+(NH_3)_{n'}$, respectively. The latter fragment contains NH_3 that presumably originated from positions off the hydroxy group, because NH_3 molecules bound to the aromatic ring would have disappeared with the phenoxy radical. We should then be able to determine where NH_3 are originally bound by comparing the time-resolved traces for $PhOH^+(NH_3)_n$ and $H^+(NH_3)_{n'}$ and comparing the minimum and maximum values of n and n' for which ESPT is evident. We know that ESPT occurs for $n \geq 5$ from the measurements in Figure 4. Under low ionization energy and in the limit of low probe pulse energy, the range of n' values that show the same time dependence is $4 \geq n' \geq 6$.[16] The difference in onset values of n and n' is only one, which can be interpreted as being due to evaporation in the product signal or to an NH_3 molecule being bound to the ring where it goes undetected in the $H^+(NH_3)_n$ signal. The former possibility is likely because evaporation is clearly evident as ionization energy and pulse energy are increased. Hence, this evidence suggests that for $n = 5$ no more than one or two NH_3 molecules bind to the ring. Alternatively, one could argue that clusters for which more than one NH_3 binds to the ring are unreactive and, therefore, do not show decay kinetics in the time dependence of reactant and product. However, this possibility is unlikely because the reactant signal $PhOH^+(NH_3)_n$ for $n \geq 5$ decays nearly to the base line, indicating that all clusters of these sizes undergo reaction. These conclusions, though not ironclad, do indicate that NH_3 prefers to bond in a hydrogen bond network off the hydroxy group rather than to the ring in phenol. This conclusion may not apply to naphthol for which the greater aromaticity may increase the hydrogen bond strength of NH_3 to the ring.

Many key questions regarding solvent structure remain unanswered: (i) where do NH_3 molecules bond in ROH−B_n clusters, (ii) how does the propensity to bind to different sites depend on number of solvent molecules, (iii) is there a greater preference for ring bonding in naphthol *vs* phenol, and (iv) how does NH_3 solvate the anion? An important start to answering these questions is to measure hydrogen bond strengths to benzene *vs* naphthalene by recording spectral shifts in excitation and dispersed fluorescence spectra and by IR−UV and Raman−UV double-resonance techniques such as those practiced by the groups of Felker, Zwier, Mikami, and others.[84−87]

Mixed Solvent Effects on ESPT. We have studied ESPT in mixed solvents involving NH_3 with CH_3OH or trimethylamine (TMA). Adding a dissimilar solvent molecule to an otherwise pure solvent cluster can cause a change in the hydrogen-bonding network that can affect chemistry dramatically. The NH_3/TMA solvent system is interesting because TMA has a much higher proton affinity than NH_3 (9.8 *vs* 8.8 eV)[75] and, therefore, a greater hydrogen bond potential; however, TMA also terminates hydrogen bond networks because the methyl groups do not undergo hydrogen bonding. Castleman and group used this property to good effect in determining the structure of water clathrates by titrating the number of dangling hydrogen bonds by TMA.[97] In our work we found that the mass spectrum for PhOH−B_n peaks strongly at $n = 1$ for TMA, but to much higher values of n for NH_3 under similar expansion conditions reflecting the hydrogen bond terminating and propagating traits of TMA and NH_3, respectively. Interestingly, in mixed NH_3/TMA, the major signal is due to PhOH−$NH_3(TMA)_3$. Even though TMA forms a much stronger bond to phenol than does NH_3 (0.56 *vs* 0.29 eV, respectively),[19,90] the cluster adopts a geometry that minimizes the overall solvent structural energy. In this case, the weaker phenol−NH_3 bond is favored because it makes available three hydrogen-bonding sites, which become occupied by TMA.

Another mixed-solvent system that strongly governs phenol reactivity is NH_3/CH_3OH.[17] Reaction rates for different solvent distributions of similar cluster size are presented in Figure 7. The substitution of a single CH_3OH molecule for an NH_3 molecule causes a substantial decrease in reaction rate. Excited phenol in neat NH_3 solvent cluster $(n,m) = (6,0)$ reacts in 65 ps whereas the (5,1) cluster reacts in 750 ps. Considering that the (5,0) cluster reacts in 60 ps (*cf.* Figure 4), the (5,1) result indicates that the *addition* of a single CH_3OH molecule quenches

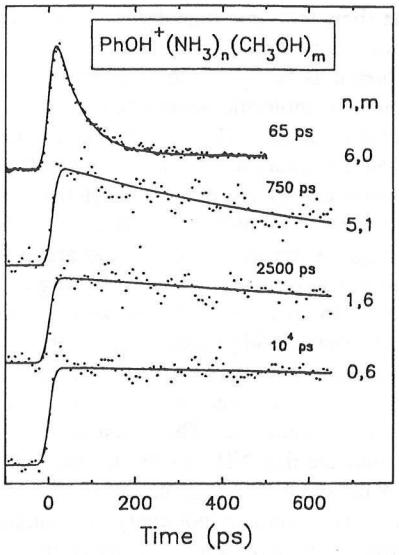

Figure 7. Picosecond measurements of $PhOH^*(NH_3)_n(CH_3OH)_m$ using 266 nm pump and 532 nm probe.

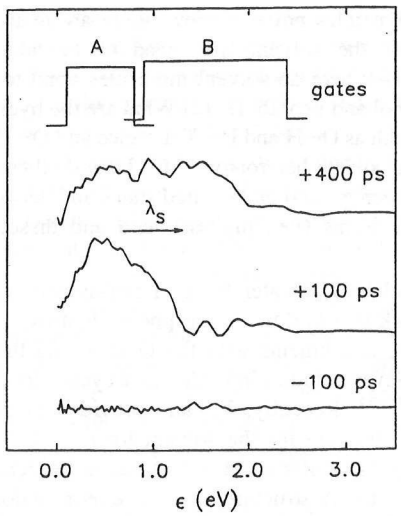

Figure 8. Time-resolved photoelectron spectra as a function of pump–probe delay time t. These plots are difference spectra corresponding to $(\lambda_1 + \lambda_2) - (\lambda_1)$.

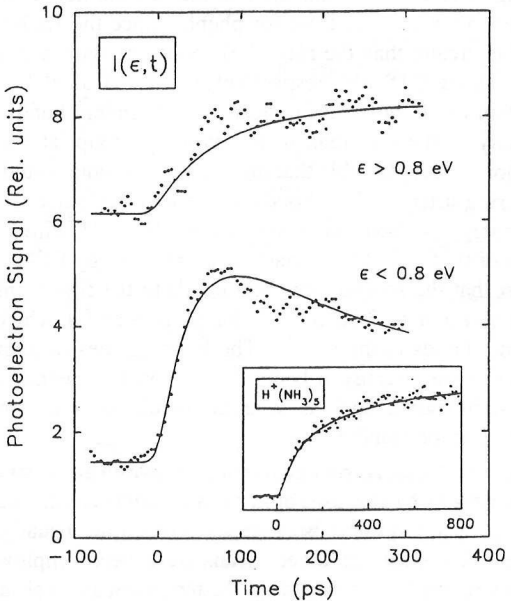

Figure 9. Observed time dependences of the low-energy (gate A) and high-energy (gate B) photoelectron bands in Figure 8. Fitted curves were calculated for rate constants $k = (50\ \text{ps})^{-1}$ and $k_s = (300\ \text{ps})^{-1}$ and spectral parameters discussed in ref 21. The insert shows the total product ion yield and is fitted to a biexponential function with time constants of 65 and 300 ps.

the reactivity of the (5,0) cluster. This is surprising because it implies that the aggregate proton affinity of the solvent is somehow reduced by the addition of CH_3OH.

The reduced reactivity in the presence of CH_3OH can be explained by solvent structure. It is known from gas-phase cluster studies that the closed-shell structure $NH_4^+(NH_3)_4$ is very favorable for stabilizing a proton.[76,98,99] However, spectroscopic and mass spectrometric evidence for the mixed NH_3/CH_3OH solvation of PhOH indicates that NH_3 forms the stronger bond to PhOH but that CH_3OH forms the stronger bond to PhOH·NH_3.[19] Indeed, the NH_3-CH_3OH bond is stronger than the NH_3-NH_3 bond.[100] Consequently, given a chance, CH_3OH will displace NH_3 from the first solvation shell and prevent a pure NH_3 solvent cluster from forming. Also, CH_3OH can form a stable hydrogen bond to the phenol oxygen which diminishes excited-state acidity, whereas NH_3 avoids that site.[101] The concept of critical solvent structures in ESPT reactions has been investigated in the solution phase by Robinson and coworkers.[46] Their picosecond measurements and theoretical analyses on aromatic acids (*e.g.*, 1- and 2-naphthol) in H_2O and alcohol (CH_3OH and C_2H_5OH) support the notion that a critical solvent cluster core is necessary to act as an efficient proton acceptor. For 2-naphthol in H_2O, the critical solvent core size is reported to be about four.[46]

3.4. Solvent Reorganization. We are discovering from clusters work that solvent structure is a crucial property in determining chemical reactivity. This explains the considerable attention given above to the static, structural properties of the solvent. Here we consider what happens to the solvent structure after reaction occurs and, in so doing, consider the dynamical properties of the solvent. When proton transfer occurs, the solvent is no longer at equilibrium. The formation of a large product dipole is expected to exert a force on the solvent leading to further dynamics. For simplicity, we consider that reaction and solvent dynamics are separable, that is

$$PhOH^*\cdots B_n \xrightarrow{k} [PhO^{*-}\cdots H^+B_n]_{ur} \xrightarrow{k_s} [PhO^{*-}\cdots H^+B_n]_r \quad (2)$$

where the subscripts "ur" and "r" denote unrelaxed and relaxed solvent configurations and k_s is the solvent reorganization rate constant (*cf.* Figure 3).

Time-Resolved Ionization Efficiency. The product formation curves we recorded in Figures 8 and 9 show two time dependences, a rapid rise matching the decay of the $PhOH^+(NH_3)_n$ signals (55–70 ps) and a much slower growth component of about 300 ps.[17,21,23] The fast time response is due to the ESPT reaction. The slow time response is ascribed to solvent cluster reorganization. For 1-naphthol$(NH_3)_n$, a two-component time dependence is observed for the excited-state decay, which is attributed similarly to ESPT and solvent reorganization. The reorganization time varied from 200 ps to 3 ns depending on excitation energy and number of NH_3 molecules.[14–16]

The manner in which the potential energy along the O–H coordinate might change with time due to solvent reorganization is illustrated qualitatively in Figure 3. We assume that the solvent structure reorganizes to achieve a configuration that best stabilizes the proton (and counterion). This reorganization or "solvation of the proton" causes delocalization of charge and lengthening of the O–H bond. The changing geometry with

time leads to a changing ionization efficiency due to a shift in the Franck–Condon (FC) distribution for ionization (*i.e.*, the product state distribution from which ionization occurs is changing with time). Consequently, the total product ion yield $H^+(NH_3)_n$, shown in the insert to Figure 9, has a fast rise due to ESPT and a slow rise attributed to solvent reorganization. The details of this simple kinetic model are given elsewhere.[17] For $PhO^{*-}H^+(NH_3)_n$, the ionization efficiency seems to increase with solvent reorganization, whereas for $1\text{-}NpO^{*-}H^+(NH_3)_n$ it apparently decreases. It would be interesting to explore whether this different behavior might be related to the possibility that NH_3 binds more favorably to the aromatic ring of naphthol relative to phenol, as surmised above.

Time-Resolved Photoelectron Spectroscopy. A more detailed probe of geometry change is obtained by monitoring the individual FC components to ionization by time-resolved photoelectron spectroscopy.[21] In Figure 8 photoelectron spectra are plotted for different probe delay times. The spectra are broad because of the distribution of cluster sizes, large density of low-frequency modes, rapid vibrational redistribution, and large geometry change upon ionization. For positive t, a low-energy photoelectron band appears. Low-energy electrons correspond to ions with high internal energy and would be the outcome of poor FC factors to ionization. However, in time, the solvent reorganizes to better solvate the proton and evolves to a geometry that apparently has better overlap with the equilibrium cluster ion geometry. This leads to more vertical FC factors for ionization and lower energy ions (*i.e.*, higher-energy electrons). This is observable in the photoelectron spectra by a band that shifts to increasing energy with time. This method is analogous to recording time-dependent Stokes shifts of emission bands in studies of solvent relaxation in the condensed phase.[102–105]

Time-dependent spectral shifts in emission bands have been used to measure solvent relaxation in condensed phase. In these experiments, the relaxation dynamics are generally related by the correlation function

$$C(t) = \frac{\nu(t) - \nu(\infty)}{\nu(0) - \nu(\infty)} \tag{3}$$

where $\nu(t)$, $\nu(0)$, and $\nu(\infty)$ are the emission maxima at time t, $t = 0$, and $t = \infty$, respectively.[102–104] $C(t)$ is predicted to decay exponentially in a pure Debye solvent with a longitudinal relaxation time constant τ_L. It is reasonable to expect that time-dependent photoelectron spectroscopy should be sensitive to similar structural dynamics in clusters.

We apply a simple model for describing the time dependence of the photoelectron spectrum by assuming that the Franck–Condon photoelectron band is a Gaussian of width σ and shifts by λ_S due to solvent reorganization.[21,104] These assumptions are not rigorous. Although the spectral shift is a function of λ_S, the actual dependence is difficult to know without knowledge of the shapes of the potential surfaces for the initial and final states involved in the photoelectron transition. Also, some solvent rearrangement might already have occurred in the reactant in order to achieve the critical configuration for reaction. The time dependence as a function of photoelectron energy ϵ is given by

$$g(\epsilon,t) = \exp\left\{-\frac{[(\epsilon_0 + \lambda_S - \epsilon) - \lambda_S \varrho(t)]^2}{\sigma^2}\right\} \tag{4}$$

where ϵ_0 is the energy of the band maximum at $t = 0$ (unrelaxed spectrum) and $\varrho(t)$ is the time dependence for the band maximum. The function $\varrho(t)$, which is equivalent to $C(t)$ in eq 3 in this simple model, is a measure of cluster relaxation along the solvent coordinate. We define $\varrho(t)$ as a decaying function [$\exp(-k_s t)$ hereafter] so that the band maximum $\epsilon_0 + \lambda_S[1 - \varrho(t)]$ is ϵ_0 at $t = 0$ and $\epsilon_0 + \lambda_S$ at $t = \infty$. For positive λ_S, the photoelectron band shifts to higher energy (*i.e.*, lower ion energy), corresponding to a red shift in terms of the product-state to ion-state transition energy. This is the predicted direction of change for a solvent cluster that undergoes a change in configuration that better resembles the equilibrium geometry of the cluster ion. Some of the assumptions of our simple model include describing the solvent modes classically by a single reorganization parameter λ_S, ignoring internal modes in the Franck–Condon distribution, assuming a constant width parameter σ with time, and assuming a constant integrated photoelectron band intensity with time.

To illustrate the expected time dependence as a function of photoelectron energy, we consider the simple case of $\epsilon = \epsilon_0$ and $\epsilon = \epsilon_0 + \lambda_S = \epsilon_\infty$. This represents the intensity at the peak positions for $t = 0$ and $t = \infty$. From eq 4, we obtain

$$g(\epsilon_0,t) = \exp\left\{-\frac{\lambda_S^2}{\sigma^2}(1 - e^{-k_s t})^2\right\} \tag{5a}$$

$$g(\epsilon_\infty,t) = \exp\left\{-\frac{\lambda_S^2}{\sigma^2}e^{-2k_s t}\right\} \tag{5b}$$

These expressions show that $g(\epsilon_0,t)$ decreases with time and $g(\epsilon_\infty,t)$ increases with time. It is easy to see that, at the asymptotic limits $t = 0$ and $t = \infty$, the intensity approaches a plateau level. The function $g(\epsilon,t)$ is sensitive to the values of ϵ, the spectral parameters λ_S and σ, and the functional form of $\varrho(t)$. Accurate determination of each of these properties can be obtained by recording a series of time-resolved measurements over narrow electron energy bands or by recording the evolving photoelectron band over narrow time intervals.

The observed time dependences in Figure 9 were fitted by the expression

$$I(\epsilon,t) = \int_{-\infty}^{\infty} f(t-t')[1 - e^{-kt'}]g(\epsilon,t')\,dt' \tag{6}$$

which includes the instrument time response and ESPT product formation kinetics. Because the time scale for these functions is much shorter than for solvent reorganization, the time dependence for the observed signal $I(\epsilon,t)$ is nearly equivalent to $g(\epsilon,t)$.

The time dependence for the low-energy and high-energy photoelectron bands (gates A and B) is plotted in Figure 9. The low-energy band (ions of high internal energy) increases rapidly in intensity and then decays at a slower rate. The high-energy band (ions of low internal energy) shows a corresponding slow rate of increase. These observations support the interpretation of a Franck–Condon distribution that changes with time due to solvent reorganization. The calculated curves in Figure 9 are based on a simple model that assumes a Gaussian photoelectron band that shifts to a new peak energy by a single-exponential rate constant k_s.[21] The fitted rate constants are $k = (50\text{ ps})^{-1}$ and $k_s = (300\text{ ps})^{-1}$, which is in excellent agreement with the time-resolved mass spectrometry results for total ion yield shown in the insert to Figure 9.

3.5. Barrier Properties and Tunneling Mechanism. The probability of proton (and electron) tunneling in the condensed phase depends strongly on solvents.[106–110] Static interactions account for the general shape of the potential energy surface and the equilibrium enthalpy of the reaction. Dynamic interac-

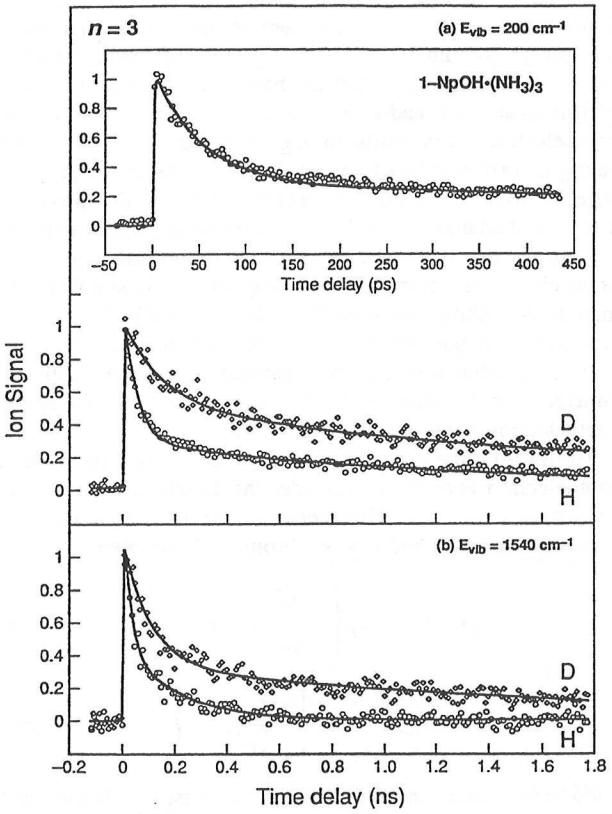

Figure 10. Femtosecond measurements of 1-NpOH*(NH$_3$)$_3$ and 1-NpOD*(ND$_3$)$_3$. (Results are from ref 15.)

tions such as solute−solvent vibrations and fluctuations in solvent orientation and lattice structure modulate the barrier width and the relative energy of the potential wells.

The barrier properties for ESPT are especially interesting in small clusters because it is not known whether a few solvent molecules act in a manner similar to condensed-phase solvents in facilitating tunneling. This raises the question, is tunneling expected to occur at all in cold clusters and, if so, by what mechanism? We recently investigated this question and obtained evidence that proton tunneling does occur in small clusters of phenol−(NH$_3$)$_n$.[2] Similar behavior has been reported by the Bernstein and Kelley group and by the Zewail group for 1-NpOH(NH$_3$)$_n$.[14−16] The principle evidence in both systems is the observation that the transfer rate for a deuteron is about an order of magnitude slower than for a proton, as seen in Figure 10.

We have been developing a model of proton tunneling in clusters that can be made applicable to condensed-phase systems in order to draw direct comparisons between these two very different solvent systems. Our model is based on concepts developed by Kelley and Bernstein *et al.*[16] but also borrows from Marcus theory[111] to include activated solvent behavior and from radiationless transition theory[112] to include a manifold of product vibrations that are Franck−Condon coupled to the motions along the reaction coordinate.

Barrier Model. To begin a model of tunneling, one must assume some barrier properties. Our picture of the barrier along the O−H coordinate in Figure 11 is based on the assertion made earlier that the potential surface and barrier to proton transfer derive from a curve crossing involving a short-range O−H covalent bonding potential and a long-range Coulombic O$^-$H$^+$ ion-pair potential (Figure 6).[17,22,23] The example shown is for a fixed O···N distances of 2.8 Å[79,82,83,113] and a fixed solvent coordinate for which the reactant and product energies are isoenergetic. On the basis of the calculated electronic splitting

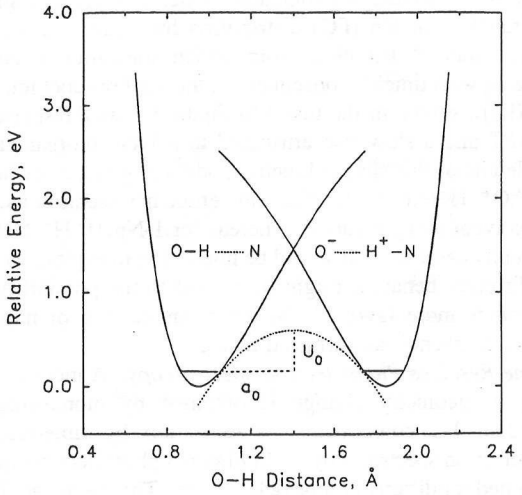

Figure 11. Barrier to ESPT arising from the crossing of a covalent and ion-pair potential for PhOH*(NH$_3$)$_5$. A parabolic function, used for the tunneling calculations, is fitted to the crossing region; a_0 and U_0 are the barrier half-width and height measured from the vibrationless level of O−H.

by Juanós i Timoneda and Hynes for the neutral and ion-pair potentials of a model OH−N complex (1 eV for an O···N distances of 2.8 Å),[108] we obtain a barrier height U_0 of 0.4 eV measured from the vibrationless level. The equilibrium barrier half-width a_0 is estimated to be 0.30 Å.[22] An important point to note is that the barrier width and height depend directly on the O···N distance. This distance depends in part on the hydrogen bond strengths involved and may explain why the rate of ESPT in 1-NpOH is faster for piperidine solvent than for NH$_3$. The former solvent forms a stronger hydrogen bond that presumably decreases the OH−N distance and, hence, barrier width to tunneling. An important dynamical solvent property affecting tunneling rates involves the role of vibrations on the barrier width. Most important is the symmetric O···N van der Waals stretch mode, which modulates a and U from their equilibrium values, leading to enormous enhancements in the tunneling probability during the compression phase of the vibration.

Tunneling Models. We adopt the method of Bernstein and Kelley *et al.* for calculating tunneling probabilities based on Bell tunneling theory and an inverted parabolic barrier[107] and integrating over the tunneling modulation caused by the O···N vibration. Bell theory assumes that tunneling occurs only when a reactant and product state become degenerate (Figure 11). Bernstein and Kelley *et al.* avoid this problem by assuming that the product potential acts as a continuum of states. Our strategy is to model the product density of states more realistically by considering a manifold of bound states and allowing the solvent fluctuations to overcome energy mismatches for tunneling resonances. In this way we can explore whether the cluster results have any similarity to bulk-solvent behavior.

Let us look at a pictorial description of tunneling to see what ingredients are important for modeling the problem. Figure 11 portrays the idealized case where reactant and product minimum energies are the same. However, this situation will exist only for specific solvent configurations that we call $S^{\ddagger}$. Other solvent configurations will break the degeneracy. It is also important to note that equilibrium solvent geometries for reactant and product, S_r and S_p, are not likely to be the same and that the O−H potential will be different for these solvent configurations as portrayed in Figure 12a. This picture implies that proton transfer cannot occur unless solvent motion occurs to reduce the energy of the product state. This in effect introduces an

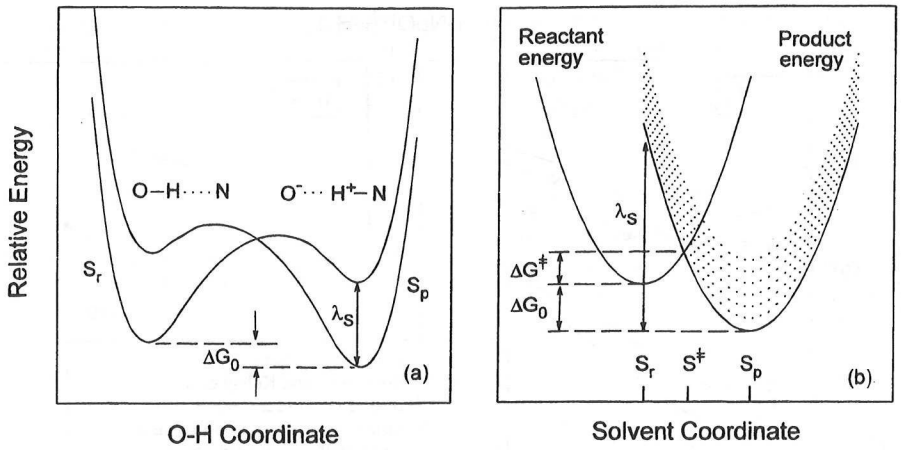

Figure 12. (a) Schematic representation of the potential energy along the O−H coordinate for fixed solvent configurations S_r and S_p. (b) Reactant and product minimum energy as a function of solvent coordinate S. $\Delta G^{\ddagger}$ is the free energy of activation for achieving resonance between the reactant and product minimum (vibrationless) energy. ΔG_0 is the free energy of reaction for an equilibrating solvent. λ_S is the solvent reorganization energy. The dotted curves represent potentials for vibrationally excited product. In the inverted region, these curves provide low activation energy pathways to product, which act to *soften* the decline of k with increasing $-\Delta G_0$.

activation energy due to the obstacle of moving solvent molecules, for example, reaching the critical solvent configuration $S^{\ddagger}$ for bringing the reactant and product minimum energies (or vibrationless levels) into resonance.[22,109,110] It is convenient to view the reactant and product minimum energies as a function of solvent coordinate as shown in Figure 12b. One then sees that there is a barrier along the solvent coordinate, which is in addition to the tunneling barrier along the O−H coordinate in Figure 11. The solvent barrier $\Delta G^{\ddagger}$ goes to zero at $\Delta G_0 = -\lambda_S$, but then it increases again as the reaction becomes more exoergic. This property predicts a decreasing reaction rate with increasing exoergicity, analogous to the Marcus inverted region for electron-transfer reactions.[111] It occurs because the energy gap between the reaction and product states becomes too large to be surmounted by energy fluctuations due to solvent motion.

The Marcus inverted region behavior is seldom observed, and that is because the reactant state does not interact with a single vibrationless product state, but a manifold of vibrationally accessible product states at energies above the minimum energy as depicted by the dotted curves in Figure 12b. If Figure 12b were drawn for the inverted region case by lowering all the product curves such that $-\Delta G_0 > \lambda_S$, then one would see that there are accessible vibrationally-excited product states for which the solvent barrier is small. In this case the drop in k in the inverted region would be more gradual. This point is very important for clusters because the temperatures are low, and one would, therefore, not expect solvent fluctuations to be able to overcome large reactant/product energy mismatches.

We are now ready to model the proton tunneling problem in clusters. A minimum of four nuclear coordinates is needed: (1) the O−H coordinate q_H, which is the reaction coordinate; (2) the O···N coordinate Q_N, in which the O···N symmetric stretch modulates the internuclear distance between potential minima, which in turn modulates the barrier height and width; (3) the solvent coordinate S, in which solvent modes cause fluctuations in the relative energies of reactant and product; and (4) coordinates corresponding to product accepting modes that reduce the electronic energy gap between reactant and product. All coordinates, except for S, are treated quantally in our treatment.[22]

It is useful to start with a Golden Rule type equation of the form

$$W_{r\to p} = (4\pi^2/h)C^2\varrho \tag{7}$$

The coupling term C is obtained from Bell theory for an O−H symmetric double-well potential with an inverted parabolic barrier as[107]

$$C = \frac{h\nu_H}{2\pi}\exp\left[-\frac{\pi^2 a}{h}(2mU)^{1/2}\right] \tag{8}$$

where $2C$ is the tunneling splitting and $2a$ and U are the barrier width and height as depicted in Figure 11. The term ϱ is the density of states for which the reactant and product are in resonance for tunneling and depends on a Boltzmann term for solvent fluctuations giving the correct solvent configuration $S^{\ddagger}$ and a manifold of product vibrational states that are Franck−Condon coupled to the reactant state. We have worked out the following expression.

$$\varrho_{\{m\}} = \frac{1}{2}\left(\frac{\beta}{\pi\lambda_S}\right)^{1/2}\sum_{n_1=0}^{\infty}\cdots\sum_{n_M=0}^{\infty}\prod_{i}^{M}|\langle m_i|n_i\rangle|^2\exp[-\beta\Delta G^{\ddagger}_{m_i,n_i}] \tag{9}$$

where M is the number of coupled modes, m_i and n_i are the number of quanta of mode i for reactant and product, respectively, β^{-1} is the energy per mode, and

$$\Delta G^{\ddagger}_{m_i,n_i} = \frac{1}{4\lambda_S}[\Delta G_0 + \lambda_S + \sum_i (n_i - m_i)h\nu_i]^2 \tag{10}$$

and the function $\varrho_{\{m\}}$ is defined as the effective density of product states coupled to reactant state $\prod_i|m_i\rangle$. The treatment of the Franck−Condon factors and their relation to the classical solvent fluctuations is important; the details can be found elsewhere.[22]

Finally, to calculate proton tunneling rate constants, the expression W is integrated over the O···N symmetric stretch vibrational wave function, which we noted above is important for modulating the barrier height and width, thus facilitating tunneling. One obtains

$$\begin{aligned} k_m &= \langle\psi_m|W(x)|\psi_m\rangle \\ &= \frac{4\pi^2}{h}\langle\psi_m|C(x)^2|\psi_m\rangle\varrho_m \\ &= \frac{4\pi^2}{h}\varrho_m\int_{-\infty}^{\infty}C(x)^2 f_m(x)\,dx \end{aligned} \tag{11}$$

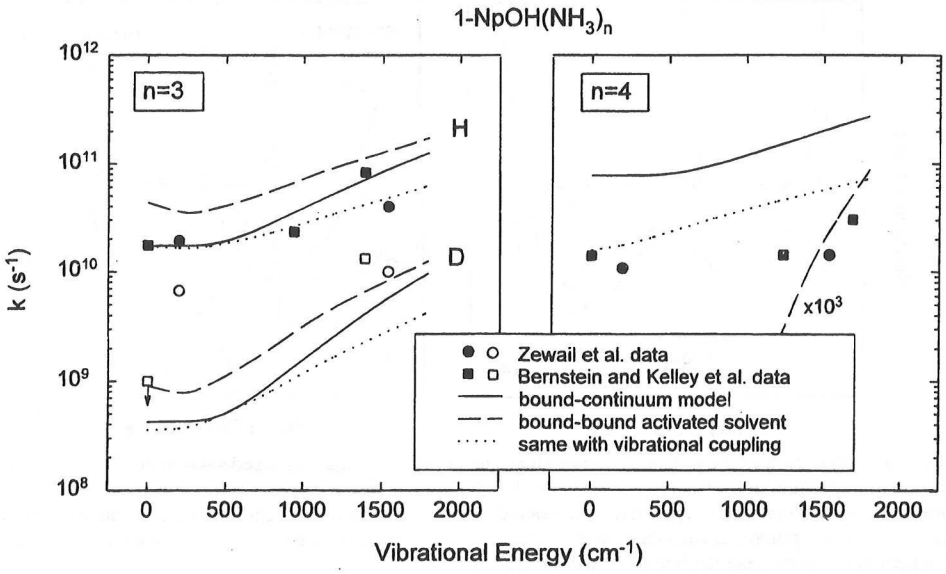

Figure 13. Calculated energy dependence of k by the three models of tunneling and comparison to measurements for 1-NpOH$(NH_3)_n$ and 1-NpOD-$(ND_3)_n$. Some parameters for calculations (n = 3 and 4, respectively) are ν_H = 3000 cm^{-1} (O−H), 2122 cm^{-1} (O−D); ν_N = 110, 99 cm^{-1}; U_0 = 0.81, 0.66 eV; a_0 = 0.214, 0.193 Å; ΔG_0 = −2200, −4700 cm^{-1}. The values of a_0 and U_0 are different for the O−H and O−D oscillators because the vibrationless levels lie at different energies. Solid and open symbols refer to protiated and deuterated clusters, respectively (cf. ref 22 for further details).

where m is the number of quanta of the O···N vibration and x is the deviation of the O···N distance from the equilibrium position. The $C(x)^2$ dependence derives from the $a(x)$ and $U(x)$ dependences and $f_m(x)$ is the O···N vibrational amplitude probability. The rate constant as a function of internal energy is then given by $k(E) = \sum_m P_m(E)k_m$ where $P_m(E)$ is the population probability of m quanta of O···N stretch at energy E. We have evaluated $P_m(E)$ using a classical expression based on the Marcus−Rice approximation.[22]

Some of the questions we are concerned with in modeling the experimental proton transfer results include the following: (1) Is the energy dependence of k attributable solely to the O−H tunneling barrier and the probability of populating the important O···N mode as assumed by the Bernstein and Kelley *et al.* model,[16] or are solvent and vibrational dynamics also important? (2) Why is k relatively invariant to n (*cf.* Figures 4 and 5 for NH_3 solvation)?

Calculations of tunneling rates were made as a function of vibrational energy E_{vib}, reaction free energy ΔG_0, and barrier properties such as width and height. Details of these calculations and comparisons with other experimental parameters are given elsewhere.[18] Calculated results are plotted against experiment for 1-naphthol$(NH_3)_n$ and phenol$(NH_3)_n$ in Figures 13 and 14. Three variations of the tunneling model are presented: (1) the bound−continuum model by Bernstein and Kelley *et al.*,[16] (2) the bound−bound activated solvent model that we developed before incorporating a manifold of coupled product vibrations, and (3) the same model, but with product vibrations included. The three model treatments use the same expressions pertaining to the isotope effect and obtain good agreement with experiment. Where the models differ is as follows: (1) The bound−continuum model predicts the relative rates as function of E_{vib} well but cannot handle the rates as a function of ΔG_0 as seen in Figures 13 and 14. (2) The solvent-activated bound−bound model is poor to adequate in handling the E_{vib} and ΔG_0 dependence. (3) The solvent-activated bound−bound model with vibrational coupling, on the other hand, gives reasonable dependences of rate on E_{vib} and ΔG_0. (4) The reorganization energy λ of about 4000 cm^{-1} used in these calculations is consistent with the value measured for phenol−ammonia clusters in Figure 8.

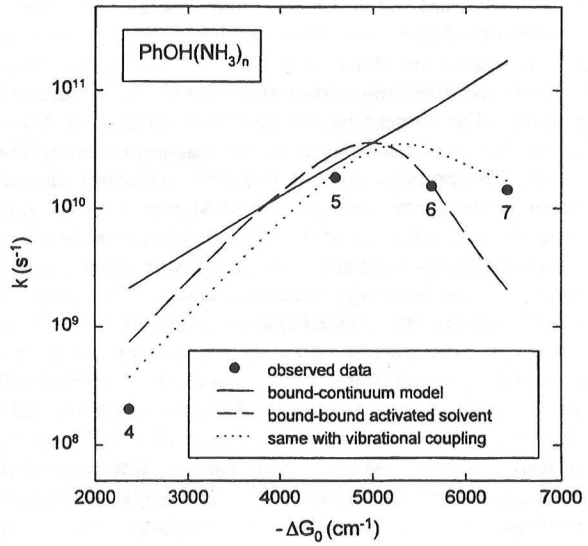

Figure 14. Calculated dependence of k on cluster size n and ΔG_0 by the three models of tunneling and comparison to measurements for PhOH$(NH_3)_n$. Some parameters for calculations (n = 4−7, respectively) are ν_H = 3500 cm^{-1}, ν_N = 140 cm^{-1}; U_0 = 0.54, 0.40, 0.335, 0.285 eV; a_0 = 0.349, 0.30, 0.275, 0.253, Å; ΔG_0 = −2360, −4600, −5640, −6440 cm^{-1} (cf. ref 22 for further details).

Figure 13 contains the most recent Zewail group measurements, which show a smaller deuteration effect and a flatter energy dependence than that reported by the Bernstein and Kelley group. The model tunneling curves were calculated before these results. Though general agreement with experiment is still good for the activated-solvent model with vibrational coupling, it would be worthwhile to reexamine the barrier properties in the model to accommodate a smaller deuteration effect. Decreasing slightly the barrier width and height would decrease the dependence of rate on deuteration and vibrational energy but would also increase the overall rates. To bring the rates back to experimental values would require evaluating the density of solvent and other modes relative to the O···N promoting mode.

Figure 14 deals with the issue of why the ESPT rates are fairly constant with increasing n, even though one expects the

reaction exoergicity or driving force to increase. One explanation is that ESPT in clusters reflects a Marcus inverted region behavior. The best fit to the $PhOH(NH_3)_n$ data in Figure 14 is based on a ΔG_0 scale that is exoergic even for $n = 4$, which is unreactive (or very slow) in our experiments. The maximum rate with n is then that which has a $-\Delta G_0$ close to the solvent reorganization energy. For larger n classical Marcus theory predicts a decrease in tunneling rate. However, because of a strongly coupled manifold of product vibrational states, this decrease in rate becomes less steep and may even saturate to a relatively constant value.

Mode Specificity? The strong accelerating effect that barrier compression has on proton tunneling suggests the possibility of observing a mode-specific reaction by direct excitation of the symmetric O···N stretch. The effectiveness will depend on the competition between the rate of vibrational relaxation *vs* tunneling. Bruehl and Hynes recently calculated vibrational relaxation rates for a model A−H···B hydrogen bond complex in polar solvent.[114] They considered the proton stretch motion (over a 2500−3500 cm^{-1} range), the proton bend (from 1000 to 1700 cm^{-1}), and the symmetric stretch (from 100 to 300 cm^{-1}). Vastly different relaxation times are calculated owing partly to the fact that each vibration is sensitive to a different mix of solvent interactions (*i.e.*, Coulombic, Lennard-Jones), which in turn vary with position and geometry of the solvent molecules. The major trend is for relaxation rate to increase steeply with decreasing vibrational frequency due to the increasing spectral density of solvent modes at lower frequency. For example, the proton stretch and the symmetric stretch are calculated to relax on the order of 10 ns and 100 fs, respectively.

These calculations would seem to rule out the possibility of observing mode-selective ESPT by direct excitation of the symmetric stretch, except that the relaxation rate may be much slower in clusters. The groups of Leutwyler[81] and Mikami[90] have assigned vibronic bands in the S_1 excitation spectra of PhOH−B (B = H_2O and NH_3) to the symmetric stretch mode. The line widths are less than a few wavenumbers, which correspond to relaxation times much greater than a picosecond. In an intriguing result, Fuke *et al.* measured the picosecond proton transfer rate in 1-azacarbazole dimer and observed a strong mode specific acceleration of rate for the symmetric intermolecular N−H···N stretch vibrations.[27] They attribute the rate increase to a mechanism by which the symmetric stretch causes a "classical detour" of the quantum tunneling pathway. We wonder whether this is instead an example of mode-specific tunneling that we predict for clusters due to barrier compression. The 1-azacarbazole dimer system certainly merits further examination. Based on all the findings above, two experiments should be done:

(1) *Vibrational relaxation rates in hydrogen-bonded clusters*: Using conventional pump−probe methods, the vibrational relaxation rates for proton stretch, proton bend, and symmetric O···N stretch should be measured in S_0 and S_1 for a variety of solvents and, until the spectra broaden out, for increasing number of solvent molecules. Time-resolved photoelectron spectroscopy might give additional information on the acceptor modes coupled to the excited mode.

(2) *Mode-specific ESPT*: One must find a case for which (i) the symmetric stretch mode in S_1 is resolved and (ii) the reaction is exoergic. By choosing a strong acid (*i.e.*, $-NO_2$-substituted phenol or naphthol) and strong base (*i.e.*, trimethylamine, piperidine), it may be possible to achieve ESPT in a 1:1 complex whose excitation spectrum is likely to be resolved.

A combination of dynamical measurements, spectroscopic and structural analysis, and theory (both electronic structure and molecular dynamics) in clusters should provide considerable detail about solvent interactions that contribute to vibrational relaxation and proton transfer and would be valuable information for comparing with similar measurements in bulk solvent systems.

4. Concluding Remarks

In the past five years size-specific time-domain studies in clusters have progressed from experimental demonstrations to detailed investigations. It is now possible to make direct comparisons between clusters, condensed phase, and gas phase for reactions such as ESPT and I_2 dissociation and recombination. What makes time-domain studies of chemistry in clusters so compelling is that most of the important results were not anticipated at the beginning of the experiments, such as the strong dependence of rate on solvent size, structure, and solvent mixture. Much has been learned from the unexpected and the surprises have pointed to interesting new lines of research.

In keeping with the exploratory nature of clusters, we take the opportunity here to speculate about some future directions and to make more general comments about the utility of studying clusters. In the area of ESPT in clusters, there are a few issues of great importance that can be tackled with current techniques. First, it is important to know the structure of multiple solvent molecules on a solute molecule such as ROH, particularly for strong bases such as NH_3, which readily promote reaction. Second, the rate of vibrational relaxation should be measured under various solvent cluster conditions. This is particularly important for promoting modes for reaction such as the O···N symmetric stretch, where a sufficiently long lifetime could lead to mode-specific tunneling in clusters. Third, it would be very valuable to extend to clusters theories used to describe chemistry in condensed phases. Because of the finite size of clusters, the solvent could be treated in much greater detail, particularly, the quantum properties of solvent mode structure and vibrational relaxation could be handled in ways not possible in condensed phases.

Stretching our scope a little, it is interesting to think about possible technology applications or at least what studies might assist in developing applications. For example, the four-level systems depicted in Figures 2 and 3 have the right properties for achieving a proton transfer laser; namely, a strong neutral excited state transition, long-lived broad-band ion-pair emission, rapid interconversion between neutral and ion-pair states in both S_0 and S_1, and well-separated absorption and emission bands. Kasha and co-workers first examined the possibility of using intramolecular proton transfer molecules such as 3-hydroxyflavone as laser dyes.[115] However, it may be possible to construct a solid-state device based on hydrogen-bonded complexes embedded in a host material that is broadly tunable in the ultraviolet when pumped by excimer or Nd:YAG harmonics.

If technology is moving toward smaller and faster, then ultrafast measurements in clusters will play a key role in understanding properties of chemistry and matter on the molecular level. The future holds many possibilities. Ultrafast studies in clusters are providing building blocks of information for understanding the correspondence between the gas phase and bulk phase. In the field of computing, technology is driven by memory storage and logic switching. One can imagine individual molecules or clusters of molecules serving as a binary device that can be optically flipped (*e.g.*, cis/trans isomerization) or an optical switch consisting of a donor/acceptor pair of molecules involving transfer of an electron or proton to form an ion-pair state. Indeed, many groups are thinking along these lines and have sophisticated notions on these ideas. The point

to be made here is that understanding these properties in clusters may provide critical information to development of these devices. It will be interesting to see how basic research using forefront technologies such as ultrafast lasers and cluster sources unfolds as an investment for technology and applications.

Acknowledgment. The work from our laboratory would not have been possible without the help of my co-workers and the technical staff at Aerospace. I thank Professors A. H. Zewail and P. M. Felker for discussions that have benefited this paper.

References and Notes

(1) Castleman, Jr., A. W.; Wei, S. *Annu. Rev. Phys. Chem.*, in press.
(2) Bernstein, E. R. *J. Phys. Chem.* **1992**, *96*, 10105.
(3) Brutschy, B. *J. Phys. Chem.* **1990**, *94*, 8637.
(4) Brumer, P.; Shapiro, M. In *Coherence Phenomena in Atoms and Molecules in Laser Fields*; Bandrauk, A. D., Wallace, S. C., Eds.; Plenum Press: New York, 1992. Bandrauk, A. D., Ed. *Molecules in Laser Fields*; Marcel Dekker: New York, 1993.
(5) Krause, J. L.; Whitnell, R. M.; Wilson, K. R.; Yan, Y.; Mukamel, S. *J. Chem. Phys.* **1993**, *99*, 6562. Shi, S.; Rabitz, H. *J. Chem. Phys.* **1990**, *364*, 2927. Tannor, D. J.; Kosloff, R.; Rice, S. A. *J. Chem. Phys.* **1986**, *85*, 5805.
(6) Zewail, A. H. *J. Phys. Chem.* **1993**, *97*, 12427.
(7) Felker, P. M.; Zewail, A. H. *Chem. Phys. Lett.* **1983**, *94*, 448, 454.
(8) Knee, J. L.; Khundkar, L. R.; Zewail, A. H. *J. Chem. Phys.* **1987**, *87*, 115.
(9) Ray, D.; Levinger, N. E.; Papanikolas, J. M.; Lineberger, W. C. *J. Chem. Phys.* **1989**, *91*, 6533. Papanikolas, J. M.; Gord, J. R.; Levinger, N. E.; Ray, D.; Vorsa, V.; Lineberger, W. C. *J. Phys. Chem.* **1991**, *95*, 8028.
(10) Papanikolas, J. M.; Vorsa, V.; Nadal, M. E.; Campagnola, P. J.; Buchenau, H. K.; Lineberger, W. C. *J. Chem. Phys.* **1993**, *99*, 8733.
(11) Willberg, D. M.; Gutmann, M.; Breen, J. J.; Zewail, A. H. *J. Chem. Phys.* **1992**, *96*, 198. Gutmann, M.; Willberg, D. M.; Zewail, A. H. *J. Chem. Phys.* **1992**, *97*, 8037, 8048.
(12) Potter, E. P.; Liu, Q.; Zewail, A. H. *Chem. Phys.* **1992**, *200*, 605. Liu, W.; Wang, J.-K.; Zewail, A. H. *Nature* **1993**, *364*, 427.
(13) Lienau, C.; Heikel, A. A.; Zewail, A. H. *Chem. Phys.* **1993**, *175*, 171.
(14) Breen, J. J.; Peng, L. W.; Willberg, D. M.; Heikal, A.; Cong, P.; Zewail, A. H. *J. Chem. Phys.* **1990**, *92*, 805.
(15) Kim, S. K.; Wang, J.-K.; Zewail, A. H. *Chem. Phys. Lett.* **1994**, *228*, 369. Kim, S. K.; Breen, J. J.; Willberg, D. M.; Peng, L. W.; Heikal, A.; Syage, J. A.; Zewail, A. H. *J. Phys. Chem.*, in press.
(16) Hineman, M. F.; Bruker, G. A.; Kelley, D. F.; Bernstein, E. R. *J. Chem. Phys.* **1992**, *97*, 3341.
(17) Steadman, J.; Syage, J. A. *J. Chem. Phys.* **1990**, *92*, 4630. Syage, J. A.; Steadman, J. *J. Chem. Phys.* **1991**, *95*, 2497.
(18) Steadman, J.; Syage, J. A. *J. Am. Chem. Soc.* **1991**, *113*, 6786. Syage, J. A.; Steadman, J. *J. Phys. Chem.* **1992**, *96*, 9606.
(19) Syage, J. A. *J. Phys. Chem.* **1991**, *95*, 10326.
(20) Steadman, J.; Fournier, E. W.; Syage, J. A. *Appl. Opt.* **1990**, *29*, 4962.
(21) Syage, J. A. *Chem. Phys. Lett.* **1993**, *202*, 227. Syage, J. A. *Z. Phys. D* **1994**, *30*, 1.
(22) Syage, J. A. *J. Phys. Chem.* **1993**, *97*, 12523. Syage, J. A. *Faraday Discuss. Chem. Soc.* **1994**, *97*, 401.
(23) Syage, J. A. In *Ultrafast Spectroscopy in Chemical Systems*; Simon, J. D., Ed.; Kluwer Academic Press: New York, 1994; p 289. Syage, J. A. In *Femtosecond Chemistry*; Manz, J., Wöste, L., Eds.; VCH Publishers: New York, 1995; p 475.
(24) Syage, J. A.; Steadman, J. *Chem. Phys. Lett.* **1990**, *166*, 159.
(25) Syage, J. A. *J. Chim. Phys.*, in press.
(26) Wei, S.; Purnell, J.; Buzza, S. A.; Stanley, R. J.; Castleman, Jr., A. W. *J. Chem. Phys.* **1992**, *97*, 9480. Wei, S.; Purnell, J.; Buzza, S. A.; Castleman, Jr., A. W. *J. Chem. Phys.* **1993**, *99*, 755.
(27) Fuke, K.; Keizo, K.; Misaizu, F.; Kaya, K. *J. Chem. Phys.* **1991**, *95*, 4074.
(28) Ionov, S. I.; Brucker, G. A.; Jaques, C.; Velachovic, L.; Wittig, C. *J. Chem. Phys.* **1992**, *97*, 9486.
(29) Soep, B.; Abbés, S.; Keller, A.; Visticot, J. P. *J. Chem. Phys.* **1992**, *96*, 440. Yamanouchi, K.; Isogai, S.; Tsuchiya, S.; Duval, M.-C.; Jouvet, C.; Benoist d'Azy, O.; Soep, B. *J. Chem. Phys.* **1988**, *89*, 2975.
(30) Scherer, N. F.; Khundkar, L. R.; Bernstein, R. B.; Zewail, A. H. *J. Chem. Phys.* **1987**, *87*, 1451. Scherer, N. F.; Sipes, C.; Bernstein, R. B.; Zewail, A. H. *J. Chem. Phys.* **1990**, *92*, 5239.
(31) Smith, J. M.; Lakshminarayan, C.; Knee, J. L. *J. Chem. Phys.* **1990**, *93*, 4475. Smith, J. M.; Zhang, X.; Knee, J. L. *J. Chem. Phys.* **1993**, *99*, 2550.
(32) Cassasa, M. P.; Stephenson, J. C.; King, D. S. *J. Chem. Phys.* **1988**, *89*, 1966.
(33) Baumert, T.; Röttgermann, C.; Rothenfusser, C.; Thalweiser, R.; Weiss, V.; Gerber, G. *Phys. Rev. Lett.* **1992**, *69*, 1512.
(34) Wittmeyer, S. A.; Kazishka, A. J.; Topp, M. R. *Chem. Phys. Lett.* **1989**, *154*, 1. Kazishka, A. J.; Shchuka, M. I.; Wittmeyer, S. A.; Topp, M. R. *J. Phys. Chem.* **1991**, *95*, 3663.
(35) Sipior, J.; Sulkes, M. *J. Chem. Phys.* **1988**, *88*, 6146. Teh, C. K.; Sipior, J.; Sulkes, M. *J. Phys. Chem.* **1989**, *93*, 5393. Arnold, S.; Sulkes, M. *J. Phys. Chem.* **1992**, *96*, 4768.
(36) Felker, P. M.; Zewail, A. H. In *Femtosecond Chemistry*; Manz, J., Wöste, L., Eds.; VCH Publishers: New York, in press. Felker, P. M. *J. Phys. Chem.* **1992**, *96*, 7844 and references therein.
(37) Côte, M. J.; Kauffman, J. F.; Smith, P. G.; McDonald, J. D. *J. Chem. Phys.* **1989**, *90*, 2864. Kauffman, J. F.; Côte, M. J.; Smith, P. G.; McDonald, J. D. *J. Chem. Phys.* **1989**, *90*, 2874.
(38) Knochenmuss, R.; Holtom, G. R.; Ray, D. *Chem. Phys. Lett.* **1993**, *215*, 188.
(39) Cheshnovsky, O.; Leutwyler, S. *J. Chem. Phys.* **1988**, *88*, 4127. Knochenmuss, R.; Cheshnovsky, O.; Leutwyler, S. *Chem. Phys. Lett.* **1988**, *144*, 317.
(40) Droz, T.; Knochenmuss, R.; Leutwyler, S. *J. Chem. Phys.* **1990**, *93*, 4520.
(41) Jouvet, C.; Lardeux-Dedonder, C.; Richard-Viard, M.; Solgadi, D.; Tramer, A. *J. Phys. Chem.* **1990**, *94*, 5041. Solgadi, D.; Jouvet, C.; Tramer, A. *J. Phys. Chem.* **1988**, *92*, 3313.
(42) Burke, M. L.; Klemperer, W. *J. Chem. Phys.* **1993**, *98*, 1797.
(43) Valentini, J. J.; Cross, J. B. *J. Chem. Phys.* **1982**, *77*, 572.
(44) Harris, C. M.; Selinger, B. K. *J. Phys. Chem.* **1980**, *84*, 1366. Ireland, J. F.; Wyatt, P. A. H. *Adv. Phys. Org. Chem.* **1976**, *12*, 131.
(45) Brucker, G. A.; Kelley, D. F. *J. Chem. Phys.* **1989**, *90*, 5243. Brucker, G. A.; Kelley, D. F. *Chem. Phys. Lett.* **1989**, *136*, 213.
(46) Lee, J.; Griffin, R. D.; Robinson, G. W. *J. Chem. Phys.* **1985**, *82*, 4920. Lee, J.; Robinson, G. W.; Webb, S. P.; Philips, L. A.; Clark, J. H. *J. Am. Chem. Soc.* **1986**, *108*, 6538.
(47) Strandjord, A. J. G.; Courtney, S. H.; Friedrich, D. M.; Barbara, P. F. *J. Phys. Chem.* **1983**, *87*, 1125. Smith, T. P.; Zakilika, K. Z.; Thakur, K.; Barbara, P. F. *J. Am. Chem. Soc.* **1991**, *113*, 4035.
(48) Pines, E.; Huppert, D.; Agmon, N. *J. Chem. Phys.* **1988**, *88*, 5620. Agmon, N.; Huppert, D.; Pines, E. *J. Chem. Phys.* **1988**, *88*, 5631.
(49) Kosower, E. M.; Huppert, D. *Annu. Rev. Phys. Chem.* **1986**, *37*, 127.
(50) Huppert, D. H.; Jayaraman, A.; Maines, Sr., R. G.; Steyert, D. W.; Rentzepis, P. M. *J. Chem. Phys.* **1984**, *81*, 5596.
(51) Webb, S. P.; Philips, L. A.; Yeh, S. W.; Tolbert, L. M.; Clark, J. H. *J. Phys. Chem.* **1986**, *90*, 5154.
(52) Brucker, G. A.; Kelley, D. F. *J. Phys. Chem.* **1988**, *92*, 3805.
(53) Chuang, T. J.; Hoffman, G. W.; Eisenthal, K. B. *Chem. Phys. Lett.* **1974**, *25*, 201.
(54) Bado, P.; Wilson, K. R. *J. Phys. Chem.* **1984**, *88* 655.
(55) Abul-Haj, N. A.; Kelley, D. F. *J. Phys. Chem.* **1987**, *91*, 5903.
(56) Harris, A. L.; Brown, J. K.; Harris, C. B. *Annu. Rev. Phys. Chem.* **1988**, *39*, 341.
(57) Zadoyan, R.; Ashjian, P.; Li, Z.; Martens, C. C.; Apkarian, V. A. *Chem. Phys. Lett.* **1994**, *218*, 504.
(58) Alexander, M. L.; Levinger, N. E.; Johnson, M. A.; Ray, D.; Lineberger, W. C. *J. Chem. Phys.* **1988**, *88*, 6200. Papanikolas, J. M.; Gord, J. R.; Levinger, N. E.; Ray, D.; Vorsa, V.; Lineberger, W. C. *J. Phys. Chem.* **1991**, *95*, 8028.
(59) Kliner, D. A. V.; Alfano, J. C.; Barbara, P. F. *J. Chem. Phys.* **1993**, *98*, 5375.
(60) Banin, U.; Waldman, A.; Ruhman, S. *J. Chem. Phys.* **1992**, *96*, 2416.
(61) Syage, J. A. *Phys. Rev. A* **1992**, *46*, 5666. Syage, J. A. *J. Phys. B* **1991**, *24*, L527.
(62) Syage, J. A. *J. Chem. Phys.* **1992**, *97*, 6085.
(63) Syage, J. A. *J. Chem. Phys.* **1990**, *92*, 1804. Syage, J. A.; Steadman, J. *Rev. Sci. Instrum.* **1990**, *61*, 1204.
(64) Syage, J. A.; Pollard, J. E.; Steadman, J. *Chem. Phys. Lett.* **1989**, *161*, 103.
(65) Müller-Dethlefs, K.; Schlag, E. W. *Annu. Rev. Phys. Chem.* **1991**, *42*, 109.
(66) Zhu, L.; Johnson, P. *J. Chem. Phys.* **1991**, *94*, 5769.
(67) Krause, H.; Neusser, H. J. *J. Chem. Phys.* **1992**, *97*, 5923. Jouvet, C.; Dedonder-Lardeux, C.; Martrenchard-Barra, S.; Solgadi, D. *Chem. Phys. Lett.* **1992**, *198*, 419. Dietrich, H.-J.; Linder, R.; Müller-Dethlefs, *J. Chem. Phys.* **1994**, *101*, 3399.
(68) Steadman, J.; Syage, J. A. *Rev. Sci. Instrum.* **1993**, *64*, 3094.
(69) Trevor, D. J.; Van Woerkom, L. D.; Freeman, R. R. *Rev. Sci. Instrum.* **1989**, *60*, 1051. Liu, G.; Barton, J. J.; Bahr, C. C.; Shirley, D. A. *Nucl. Instrum. Methods* **1986**, *A246*, 504.
(70) Kruit, P.; Read, F. H. *J. Phys. E* **1983**, *16*, 313.
(71) Rademann, K.; Rech, T.; Kaiser, B.; Even, U.; Hensel, F. *Rev. Sci. Instrum.* **1991**, *62*, 1932.
(72) Cyr, D. M.; Bishea, G. A.; Scarton, M. G.; Johnson, M. A. *J. Chem. Phys.* **1992**, *97*, 5911. Cyr, D. M.; Posey, L. A.; Bishea, G. A.; Han, C.-C.; Johnson, M. A. *J. Am. Chem. Soc.* **1991**, *113*, 9697.

(73) Forster, T. *Z. Electrochem.* **1950**, *54*, 531. Weller, A. *Z. Electrochem.* **1952**, *56*, 662.

(74) Pross, A.; Radom, L.; Taft, R. W. *J. Am. Chem. Soc.* **1980**, *45*, 818.

(75) Lias, S. G.; Liebman, J. F.; Levin, R. D. *J. Phys. Chem. Ref. Data* **1984**, *13*, 695.

(76) Kebarle, P. *Annu. Rev. Phys. Chem.* **1977**, *28*, 445. Grimsrud, E. P.; Kebarle, P. *J. Am. Chem. Soc.* **1973**, *95*, 7939. Mautner, M. J.; Speller, C. V. *J. Phys. Chem.* **1986**, *90*, 6616.

(77) Deakyne, C. A. *J. Phys. Chem.* **1986**, *90*, 6625.

(78) Champagne, B. B.; Pfanstiel, J. F.; Plusquellic, D. F.; Pratt, D. W.; van Herpen, W. M.; Meerts, W. L. *J. Phys. Chem.* **1990**, *94*, 6.

(79) Plusquellic, D. F.; Tan, X.-Q.; Pratt, D. W. *J. Chem. Phys.* **1992**, *96*, 8026.

(80) Peteanu, L. A.; Levy, D. H. *J. Phys. Chem.* **1988**, *92*, 6554.

(81) Schütz, M.; Bürgi, T.; Leutwyler, S.; Fischer, T. *J. Chem. Phys.* **1993**, *98*, 3763.

(82) Connell, L. L. Ph.D. Thesis, University of California, Los Angeles, 1992.

(83) We estimate a value of 2.8 Å for the O···N bond distance for the excited state of PhOH−NH_3 and NpOH−NH_3 based on an average of different values. In ref 113, an H−N distance of 1.8 Å is reported, to which the standard O−H distance of 9.5 Å gives 2.75 Å. In ref 79 2-NpOH-(NH_3) is reported to be about 2.6 Å; however, this is being reanalyzed and is considered to be about 2.8−2.9 Å. In ref 82, a value for 1-NpOH(NH_3) of about 2.9 Å is obtained. We have not considered the affect of several solvent molecules on the O···N distance.

(84) Venturo, V. A.; Maxton, P. M.; Felker, P. M. *J. Phys. Chem.* **1992**, *96*, 5234.

(85) Pribble, R. N.; Zwier, T. S. *Faraday Discuss. Chem. Soc.* **1994**, *97*, 229.

(86) Tanabe, S.; Ebata, T.; Fujii, M.; Mikami, N. *Chem. Phys. Lett.* **1993**, *215*, 347. Fujii, A.; Sawamura, T.; Tanabe, S.; Ebata, T.; Mikami, N. *Chem. Phys. Lett.* **1994**, *225*, 104.

(87) (a) Hartland, G. V.; Henson, B. F.; Venturo, V. A.; Felker, P. M. *J. Phys. Chem.* **1992**, *96*, 1164. (b) Personal communication with P. M. Felker.

(88) Lipert, R. J.; Colson, S. D. *J. Phys. Chem.* **1990**, *94*, 2358. Lipert, R. J.; Colson, S. D. *J. Chem. Phys.* **1988**, *89*, 4579. Lipert, R. J.; Bermudez, G.; Colson, S. D. *J. Phys. Chem.* **1988**, *92*, 3801.

(89) Fuke, K.; Kaya, K. *Chem. Phys. Lett.* **1983**, *94*, 97.

(90) Mikami, N.; Okabe, A.; Suzuki, I. *J. Phys. Chem.* **1988**, *92*, 1858. Mikami, N.; Suzuki, I.; Okabe, A. *J. Phys. Chem.* **1987**, *91*, 5242.

(91) Ceyer, S. T.; Tiedemann, P. W.; Mahan, B. H.; Lee, Y. T. *J. Chem. Phys.* **1979**, *70*, 14. Greer, J. C.; Ahlrichs, R.; Hertel, V. *Chem. Phys.* **1989**, *133*, 191.

(92) Kim, S. K.; Li, S.; Bernstein, E. R. *J. Chem. Phys.* **1991**, *95*, 3119.

(93) Garvey, J. F.; Peifer, W. R.; Coolbaugh, M. T. *Acc. Chem. Res.* **1991**, *24*, 48.

(94) Stace, A. J. *J. Am. Chem. Soc.* **1985**, *107*, 755. Stace, A. J.; Shukla, A. K. *J. Phys. Chem.* **1982**, *86*, 865.

(95) Syage, J. A. *J. Phys. Chem.* **1989**, *93*, 170.

(96) Alexander, M. L.; Johnson, M. A.; Levinger, N. E.; Lineberger, W. C. *Phys. Rev. Lett.* **1986**, *57*, 976.

(97) Shi, Z.; Wei, S.; Ford, J. V.; Castleman, Jr., A. W. *Chem. Phys. Lett.* **1992**, *200*, 142.

(98) Wei, S.; Tzeng, W. B.; Castleman, Jr., A. W. *J. Chem. Phys.* **1990**, *92*, 332. Shinohara, H.; Nishi, N. *Chem. Phys. Lett.* **1987**, *141*, 292.

(99) Price, J. M.; Crofton, M. W.; Lee, Y. T. *J. Phys. Chem.* **1991**, *95*, 2182.

(100) Pimentel, G. C.; McClellan, A. L. *The Hydrogen Bond*; W. H. Freeman: San Francisco, 1960. Dykstra, C. E. *J. Phys. Chem.* **1990**, *94*, 6948.

(101) Gonohe, N.; Abe, H.; Mikami, N.; Ito, M. *J. Phys. Chem.* **1985**, *89*, 3642. Oikawa, A.; Abe, H.; Mikami, N.; Ito, M. *J. Phys. Chem.* **1983**, *87*, 5083.

(102) Maroncelli, M.; MacInnis, J.; Fleming, G. R. *Science* **1989**, *243*, 1674. Simon, J. D. *Acc. Chem. Res.* **1988**, *21*, 128.

(103) Barbara, P. F.; Walker, G. C.; Smith, T. P. *Science* **1992**, *256*, 975.

(104) Kozik, M.; Sutin, N.; Winkler, J. R. *Coord. Chem. Rev.* **1990**, *97*, 23. Jarzeba, W.; Walker, G. C.; Johnson, A. E.; Kahlow, M. A.; Barbara, P. F. *J. Phys. Chem.* **1988**, *92*, 7039.

(105) Rothenberger, G.; Negus, D. K.; Hochstrasser, R. M. *J. Chem. Phys.* **1983**, *79*, 5360. Su, S.-G.; Simon, J. D. *J. Chem. Phys.* **1988**, *89*, 908.

(106) Rentzepis, R. M.; Barbara, P. F. *Adv. Chem. Phys.* **1981**, *47*, 627.

(107) Bell, R. P. *The Tunnel Effect in Chemistry*; Chapman-Hall: New York, 1980; Chapter 2.

(108) Juanós, i Timoneda, J.; Hynes, J. T. *J. Phys. Chem.* **1991**, *95*, 10431.

(109) Borgis, D. C.; Lee, S.; Hynes, J. T. *Chem. Phys. Lett.* **1989**, *162*, 19. Borgis, D. C.; Hynes, J. T. *Chem. Phys.* **1993**, *170*, 315. Borgis, D. C.; Hynes, J. T. *J. Chem. Phys.* **1991**, *94*, 3619.

(110) Cukier, R. I.; Morillo, M. *J. Chem. Phys.* **1990**, *91*, 857. Morillo, M.; Cukier, R. I. *J. Chem. Phys.* **1990**, *92*, 4833. Makri, N.; Miller, W. H. *J. Chem. Phys.* **1989**, *91*, 4026.

(111) Marcus, R. A. *Faraday Discuss. Chem. Soc.* **1982**, *74*, 7. Marcus, R. A. *Annu. Rev. Phys. Chem.* **1964**, *15*, 155. Closs, G. L.; Miller, J. R. *Science* **1988**, *240*, 440.

(112) Jortner, J.; Bixon, M. *J. Chem. Phys.* **1988**, *88*, 167. Ulstrup, J.; Jortner, J. *J. Chem. Phys.* **1975**, *63*, 4358. Freed, K. F. *Acc. Chem. Res.* **1978**, *11*, 74.

(113) Matsuyama, A.; Imamura, A. *Bull. Chem. Soc. Jpn.* **1972**, *45*, 2196.

(114) Bruehl, M.; Hynes, J. T. *Chem. Phys.* **1993**, *175*, 205.

(115) Parthenopoulos, D. A.; Kasha, M. *Chem. Phys. Lett.* **1988**, *146*, 77.

JP943135Y